

Precessing Binary Black Holes Simulations: Quasicircular Initial Data

Abdul H. Mroué¹ and Harald P. Pfeiffer¹

¹*Canadian Institute for Theoretical Astrophysics, 60 St. George Street, University of Toronto, Toronto, ON M5S 3H8, Canada*
(Dated: October 11, 2012)

In numerical evolutions of binary black holes (BBH) it is desirable to easily control the orbital eccentricity of the BBH, and the number of orbits completed by the binary through merger. This paper presents fitting formulae that allow to choose initial-data parameters for generic precessing BBH resulting in an orbital eccentricity $\sim 10^{-4}$, and that allow to predict the number of orbits to merger. We further demonstrate how these fits can be used to choose initial-data parameters of desired non-zero eccentricity. For both usage scenarios, no costly exploratory BBH evolutions are necessary, but both usage scenarios retain the freedom to refine the fitted parameters further based on the results of BBH evolutions. The presented fitting formulas are based on 729 BBH configurations which are iteratively reduced to eccentricity $\lesssim 10^{-4}$, covering mass-ratios between 1 and 8 and spin-magnitude up to 0.5. 101 of these configurations are evolved through the BBH inspiral phase.

PACS numbers: 04.25.D-, 04.25.dg, 04.25.Nx, 04.30.-w, 04.30.Db

I. INTRODUCTION

The next generation of gravitational-wave detectors, such as advanced LIGO, VIRGO and KAGRA [1–5] is under construction. These advanced detectors will have an order of magnitude increase in their sensitivity and are widely expected to make the first direct detections of gravitational waves by sources such as coalescing compact object binaries. The ability to detect and study these systems depends on the quality and accuracy of the theoretical waveform models used in building search templates for these detectors.

After breakthroughs in numerical relativity [6], direct numerical calculation of the signal emitted during the last phase of the binary’s life have become available and have been rapidly improving (e.g. [7, 8]). These numerical waveforms guide analytical modelers and data analysts in the construction of analytical templates [9–17] and are used to assess the properties of gravitational wave data-analysis pipelines [17, 18].

The parameter space for numerical studies of binary black holes is seven dimensional: Mass-ratio, and the two spin-vectors of the two black holes. The total mass scales out due to the scale invariance of the vacuum Einstein equations, and eccentricity is expected to be radiated away during the preceding gravitational-wave driven inspiral [19, 20]. Moreover, simulations for gravitational wave data-analysis need to cover a large number of inspiral orbits and have sufficient accuracy (e.g. the recent review [21]). These requirements increase the computational cost of BBH simulations and limits the number of simulations that can be performed. Therefore, BBH simulations have generally focused on lower-dimensional subspaces of the entire BBH parameter space, for instance non-spinning systems, or systems with spins aligned with the angular momentum. For example, the number of distinct BBH parameters configurations used in Ninja-2 [17] was 29: 6 configurations with non-spinning black holes, and 20 with aligned spins (some configurations were com-

puted independently by several groups for a total of 40 numerical simulations). Numerical simulations of non-precessing BBH systems are also much more carefully studied, e.g. [22–36].

Furthermore, most of the work done to compute analytical waveform models focuses on non-precessing binaries [10, 13, 16, 37–44]. Significantly less work has been done in trying to understand dynamics of precessing binaries and the resulting waveforms, and how the numerical data agrees with the analytical approximations [45–52].

The first step for evolving a precessing system requires low-eccentricity initial data, since the orbit of a isolated binary circularizes during the inspiral via the emission of gravitational waves [19, 20]. Even binaries starting with some eccentricity at the beginning of their evolution are expected to have a negligible eccentricity near the merger phase, when the emitted signal enters the frequency band of these ground-based detectors.

In a numerical relativity simulation of the inspiral of binary black holes, the eccentricity is predetermined by three free parameters in the initial data: the orbital frequency Ω_0 , the separation between the holes r_0 and the radial velocity \dot{r}_0 (we often use the dimensionless expansion factor $\dot{a}_0 \equiv \dot{r}_0/r_0$). When initial data is constructed with the assumption of circular orbits, the resulting trajectories have an orbital eccentricity of the order one percent [53–55]. This eccentricity arises by neglecting the small, but non-zero, radial velocity and the initial relaxation of the black holes.

A variety of eccentricity definitions are given in the analytical literature [56–62] as well as in numerical relativity [53–55, 63–66]. All of these definitions employ residual oscillations in the orbital variables such as the orbital frequency, proper horizon separation and coordinate separation to estimate the eccentricity. Several methods are introduced to choose initial-data parameters that result in lower eccentricity. The evolution of post-Newtonian equations was used to find quasi-circular

parameters for the trajectories of binaries [63]. More recently, iterative procedures were developed to remove eccentricity from the initial data [54, 66–69]. These methods first utilize post-Newtonian (PN) information to find initial data with reasonably low eccentricity. The initial data is evolved for about two to three orbits, and after analyzing the orbit, the initial-data parameters are corrected to reduce the orbital eccentricity. Using these new initial-data parameters, the procedure is repeated until the desired value of eccentricity is obtained. For non-precessing binaries, the method using proper horizon separation worked well in reducing the eccentricity of binaries [30, 33, 70]. For precessing binaries, a new method was introduced in Ref. [66] which uses the instantaneous orbital frequency to reduce the eccentricity to below 10^{-4} in about four iterations.

Iterative eccentricity removal works well [66], however, it introduces extra steps into the numerical simulation of BBH systems. The goal of this paper is to deal with eccentricity removal for conformally flat BBH systems once and for all: We systematically apply the eccentricity removal procedure to a large number of different BBH systems of different mass-ratios, spin-magnitudes and spin-directions. We cover mass-ratios between 1 and 8, and spin-magnitudes up to 0.5. We then perform fits that will allow us to predict low-eccentricity initial-data parameter for BBH systems with any spin-orientations. As we show, these fits result in initial conditions with remaining eccentricity of $\sim 10^{-4}$. This is quite likely sufficient for all near-term GW data-analysis purposes [71]. These low-eccentricity fits can also be used to predict initial data parameters of a desired non-zero eccentricity. Finally, we evolve 101 of the 729 low-eccentricity initial data sets through their entire inspiral, and use this information to prepare a fitting formula that allows us to predict the number of inspiral orbits for generic BBH binaries.

This paper is organized as follows: In Sec. II, we discuss eccentricity and motivate a new definition of eccentricity, e_R , that uses the radial velocity in addition to the orbital frequency. Once low-eccentricity parameters are known, e_R allows us to estimate the eccentricity of any parameter choice nearby without evolving the initial data. In Sec. III, we quasi-circularize iteratively 729 BBH configuration with different mass-ratios, spin-magnitudes and -orientations, and various initial separations. Three of these simulations are used to compare our newly defined eccentricity e_R to the standard eccentricity based on the orbital frequency, e_Ω , used in Ref. [66]. Section IV introduces fitting formulae to the low-eccentricity configurations, and demonstrates their efficiency and their advantages over post-Newtonian formulas. In Sec. V, we provide formulas for generating initial-data parameters that result in evolutions of a predetermined eccentricity, and assess the quality of these formulas. Finally, we summarize our conclusions in Sec. VI.

II. DEFINING AND REDUCING ECCENTRICITY

A. Newtonian dynamics

For two bodies on a Newtonian orbit with small eccentricity e , the distance $r(t)$ between their centers and the orbital frequency $\Omega(t)$ can be written as

$$r(t) = \bar{r} [1 - e \sin(\bar{\Omega}t + \phi_0)] + \mathcal{O}(e^2), \quad (1)$$

$$\Omega(t) = \bar{\Omega} [1 + 2e \sin(\bar{\Omega}t + \phi_0)] + \mathcal{O}(e^2). \quad (2)$$

Here \bar{r} is the average separation, $\bar{\Omega}$ is the average orbital frequency and ϕ_0 is a phase component. Taking a time-derivative of Eqs. 1 and 2, we find

$$\dot{r}(t) = -\bar{r} e \bar{\Omega} \cos(\bar{\Omega}t + \phi_0) + \mathcal{O}(e^2), \quad (3)$$

$$\dot{\Omega}(t) = 2e \bar{\Omega}^2 \cos(\bar{\Omega}t + \phi_0) + \mathcal{O}(e^2). \quad (4)$$

Note that the factor $\bar{\Omega}^2$ is the product of the average orbital frequency $\bar{\Omega}$ and the frequency of the oscillations in $\Omega(t)$. In Newtonian gravity, these two frequencies agree.

For *circular* orbits, the distance between the Newtonian masses r_0 and their orbital frequency Ω_0 are related by Kepler's law,

$$r_0^3 \Omega_0^2 = Gm \quad (5)$$

where m is the total mass of the binary, and G represents Newton's constant which we will henceforth set equal to unity. In this case, eccentricity e and radial velocity $\dot{r}(t)$ are both identically zero.

Let us consider how small perturbations in orbital separation, orbital frequency and radial velocity will affect the eccentricity of the originally circular orbit. To accomplish this, we relate a circular orbit with r_0 and Ω_0 with a slightly eccentric orbit given by Eqs. (1) and (2). At time $t = 0$, we set $r(0) = r_0 + \Delta r$, $\Omega(0) = \Omega_0 + \Delta\Omega$, and we set a radial velocity $\dot{r}(0) = \Delta\dot{r}$. The perturbed orbit will in general have an average distance \bar{r} different from r_0 , and an average orbital frequency $\bar{\Omega}$ different from Ω_0 . We write

$$\bar{r} = r_0 + \delta\bar{r}, \quad \bar{\Omega} = \Omega_0 + \delta\bar{\Omega}. \quad (6)$$

Kepler's third law Eq. (5) is also valid for \bar{r} and $\bar{\Omega}$, and from it follows

$$\frac{\delta\bar{r}}{r_0} = -\frac{2}{3} \frac{\delta\bar{\Omega}}{\Omega_0} \equiv \epsilon. \quad (7)$$

The change $\delta\bar{r}$ and $\delta\bar{\Omega}$ are thus determined by one small parameter ϵ , which is as of yet undetermined. To proceed we substitute Eq. (6) into Eqs. (1)–(3), evaluate these expressions at $t = 0$, and equate to the assumed perturbations:

$$r_0 + \Delta r = (1 + \epsilon)r_0(1 - e \sin \phi_0)r_0, \quad (8)$$

$$\Omega_0 + \Delta\Omega = (1 - 3\epsilon/2)(1 + 2e \sin \phi_0)\Omega_0, \quad (9)$$

$$\Delta\dot{r} = -(1 + \epsilon)r_0(1 - 3/2\epsilon)\Omega_0 e \cos \phi_0. \quad (10)$$

To first order in ϵ and e , these equations simplify to

$$\frac{\Delta r}{r_0} = \epsilon - e \sin \phi_0, \quad (11)$$

$$\frac{\Delta \Omega}{\Omega_0} = -\frac{3}{2}\epsilon + 2e \sin \phi_0, \quad (12)$$

$$\Delta \dot{r} = -r_0 \Omega_0 e \cos \phi_0. \quad (13)$$

Inverting Eqs. (11)–(13) yields

$$e = \sqrt{\left(2\frac{\Delta \Omega}{\Omega_0} + 3\frac{\Delta r}{r_0}\right)^2 + \left(\frac{\Delta \dot{r}}{r_0 \Omega_0}\right)^2}, \quad (14)$$

$$\epsilon = 2\frac{\Delta \Omega}{\Omega_0} + 4\frac{\Delta r}{r_0}, \quad (15)$$

$$\tan \phi_0 = -\frac{3\Omega_0 \Delta r + 2r_0 \Delta \Omega}{\Delta \dot{r}}. \quad (16)$$

To summarize, perturbing a circular Newtonian orbit by Δr , $\Delta \Omega$ and $\Delta \dot{r}$ results in an orbit with eccentricity (14); the perturbed orbit has an average radius larger by $\delta \bar{r}/r = \epsilon$ relative to the the circular, unperturbed orbit.

B. Numerical relativity

Let us now consider general relativistic BBH binaries computed by numerical simulations. As in earlier work [65, 66] we define eccentricity based on periodic oscillations of the separation of the binary or the orbital frequency, carrying over the Newtonian definitions. Specifically, the instantaneous orbital frequency $\Omega(t)$ and the distance $r(t)$ are calculated from the coordinate motion of the apparent horizons' centers. We define their relative separation vector $\mathbf{r}(t) = \mathbf{c}_1(t) - \mathbf{c}_2(t)$ with magnitude $r(t) = |\mathbf{r}(t)|$, where $\mathbf{c}_i(t)$ are the coordinates of the center of each black hole. Using standard Euclidean vector calculus, the instantaneous orbital frequency is then computed as

$$\Omega(t) = \frac{\mathbf{r}(t) \times \dot{\mathbf{r}}(t)}{r^2(t)}, \quad (17)$$

where $\Omega(t)$ is its magnitude.

A compact binary inspiral starts at $t = 0$ with an initial separation r_0 , an orbital frequency Ω_0 and a radial velocity \dot{r}_0 . The time derivative of the orbital frequency $\dot{\Omega}(t)$ is computed and fitted with the functional form

$$\dot{\Omega}_{\text{NR}}(t) = S_{\Omega, \text{fit}}(t) + B_{\Omega} \cos(\Omega_r t + \phi). \quad (18)$$

The first part of the fit, $S_{\Omega, \text{fit}}(t)$, is a non-oscillatory function that captures the radiation-reaction driven inspiral. The second part captures the oscillatory contribution of the orbital eccentricity using fitting parameters B_{Ω} , Ω_r and ϕ . Note that the sinusoidal frequency in Eq. 18 is given by the radial frequency Ω_r . In general relativity, the orbital frequency Ω exceeds the radial frequency Ω_r

causing periastron advance [65]. With the fitted parameter B_{Ω} equal to $2e\Omega\Omega_r$ (cf. the comment after Eq. 4), we can derive updating formulas based on $\dot{\Omega}(t)$ [66]:

$$\dot{a}_0 \rightarrow \dot{a}_0 + \frac{B_{\Omega}}{2\Omega_0} \cos \phi, \quad (19)$$

$$\Omega_0 \rightarrow \Omega_0 - \frac{B_{\Omega}\Omega_r}{4\Omega_0^2} \sin \phi, \quad (20)$$

where B_{Ω} and ϕ are fitted for while Ω_0 and r_0 are given by the initial data. In Eq. (19), we have introduced the expansion factor $\dot{a}_0 = \dot{r}_0/r_0$ which appears naturally in our formulation of the initial-value problem for BBH binaries with radial velocity [54]. We use Eqs. (19) and (20) to reduce eccentricity iteratively for every simulation in this paper. Using the fitted B_{Ω} and Ω_r in addition to Ω_0 , we estimate the eccentricity e_{Ω} as

$$e_{\Omega} = \frac{B_{\Omega}}{2\Omega_0\Omega_r} \quad (21)$$

Equation (14) gives the eccentricity of a Newtonian orbit that differs by $\Delta \Omega$ and $\Delta \dot{r}$ from being circular. If we know non-eccentric initial data parameters $\Omega_{0, e=0}$ and $\dot{a}_{0, e=0}$, we can use the deviations from the $e = 0$ parameters to define eccentricity:

$$e_{\text{R}} \equiv \left[\left(\frac{\dot{a}_0 - \dot{a}_{0, e=0}}{\Omega_0} \right)^2 + \left(2 \frac{\Omega_0 - \Omega_{0, e=0}}{\Omega_c} \right)^2 \right]^{1/2}. \quad (22)$$

We will test this formula in Sec. III, and use it in Sec. V to propose a technique to construct BBH initial-data with specified non-zero eccentricity.

III. LOW-ECCENTRICITY BBH PARAMETERS

Our goal is to compute several hundred low eccentricity initial-data sets for subsequent evolutions. We proceed in two stages: In stage 1, we circularize 69 binaries by starting with post-Newtonian estimates for the initial orbital frequency and radial velocity. We perform three to four levels of iterative eccentricity removal. We use the low-eccentricity initial data parameters to generate fitting formulae that predict low-eccentricity initial data parameters for other choices of masses and spins. In stage 2, we use these fitting formulae to compute 660 additional BBH configurations, which we find have an average eccentricity of about 0.003, i.e. a factor of ~ 5 below the first stage simulations. We finally apply iterative eccentricity removal to the stage 2 simulations until the eccentricity is less than 0.001.

A. Numerical methods

We construct BH–BH initial data using the conformal thin sandwich formalism [72, 73] with quasi-equilibrium

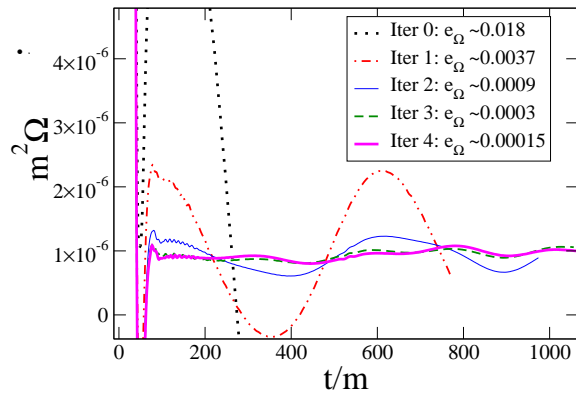


FIG. 1: **Eccentricity removal based on time derivative of the orbital frequency $d\Omega/dt$** , applied to a precessing binary black hole, ScN 21. Shown is $\dot{\Omega}$ vs. time and four eccentricity-removal iterations.

boundary conditions [74–76] and a radial velocity as in Ref. [54]. All initial-data sets considered here use conformal flatness and maximal slicing. The resulting set of five nonlinear coupled elliptic equations is solved with multi-domain pseudo-spectral techniques described in Ref. [77] implemented in the Spectral Einstein Code SpEC [78]. Calculation of initial data with desired physical parameters (masses m_A, m_B and dimensionless spins $\vec{\chi}_A, \vec{\chi}_B$) requires a root-finding procedure to determine the corresponding initial data parameters (radii of the excision boundaries r_A, r_B and angular velocities of the horizons, $\vec{\Omega}_A$ and $\vec{\Omega}_B$). This root-finding is described in Ref. [36].

The initial data is evolved with SpEC [78], using a first-order representation [79] of the generalized harmonic system [6, 80, 81] that includes constraints damping terms [6, 79, 82]. Constraint damping parameters are chosen as in [36], based on experience gathered in [30]. The computational domain extends from excision boundaries located just inside each apparent horizon to some large radius, where the outgoing gravitational radiation pass freely through the outer boundary. Outer boundary conditions [79, 83, 84] are imposed to prevent the influx of constraint violations [85–91] and undesired incoming gravitational radiation [92, 93], while no boundary conditions are imposed at the inner excision boundaries. Inter-domain boundary conditions are enforced with a penalty method [94, 95]. The overall evolution techniques (constraint damping parameters, choice of domain decomposition) are essentially identical to the inspiral phase of Ref. [36]. For precessing runs, we employ a coordinate transformation based on pitch- and yaw-angles (i.e. two of the Euler angles), described in detail in a forthcoming publication [96]. This technique works well for moderate precession as in the cases presented here, although in future runs, it will be replaced by the more sophisticated coordinate transformations developed in [96].

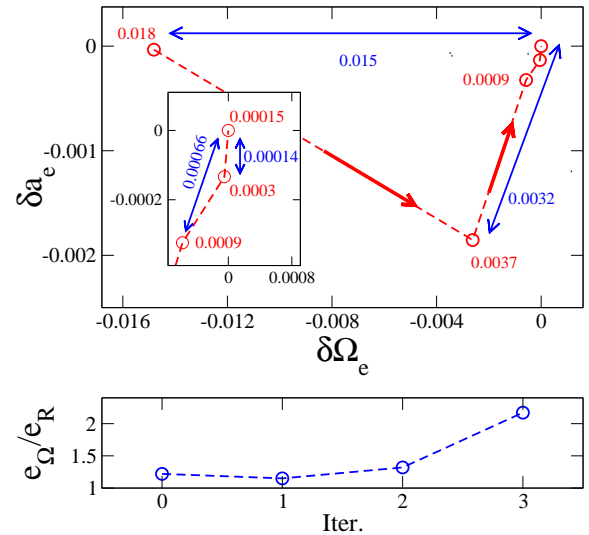


FIG. 2: **Convergence of the eccentricity-removal procedures in the $(\delta\Omega_e, \delta a_e)$ plane.** In the upper panel, we show the eccentricity removal sequence of Fig. 1. The red number next to each point gives the eccentricity e_Ω , while the blue number next to each blue solid line gives the relative eccentricity e_R . In the lower panel, we plot the eccentricities ratio e_Ω/e_R .

B. Iterative Eccentricity Reduction

We shall start by describing eccentricity removal for one typical precessing configuration, labeled ScN 21. This configuration has a mass-ratio of $q = m_A/m_B = 1.5$ and both black holes have dimensionless spins 0.5 initially tangent to the orbital plane. The spin of the larger black hole points exactly away from the smaller black hole, whereas the spin of the smaller black hole is anti-aligned with its initial velocity. The initial co-ordinate separation between the holes is $r = 16m$. We begin eccentricity removal with orbital parameters determined from a non-spinning PN approximant to choose $\Omega_0 = 0.014427/m$, and we use a previous good approximation for $\dot{a}_0 = -3.6 \times 10^{-5}$ from other simulations.

We evolve the binary with the initial orbital parameters (Ω_0, \dot{a}_0) for about two orbits, and record the time-derivative of the orbital frequency, $\dot{\Omega}(t)$. This data is plotted in Fig. 1 as “Iter 0” and we deduce an eccentricity of $e_\Omega \sim 0.018$. Equations (19) and (20) give the improved values for Ω_0 and \dot{a}_0 to use in next iteration, labeled “Iter 1” in Fig. 1 with eccentricity $e_\Omega = 0.0037$. This procedure is repeated three more times until a final eccentricity $e_\Omega \sim 1.5 \times 10^{-4}$ is achieved. Note that as the eccentricity falls below $e \lesssim 0.001$, spin-induced oscillations become apparent at twice the orbital frequency, as discussed in Ref.[66]. The spin-induced oscillation dominate for $e \lesssim 0.0003$, making unambiguous determination of a residual orbital eccentricity difficult.

Equation (22) indicates that the eccentricity is the square sum of two components, with one measuring the

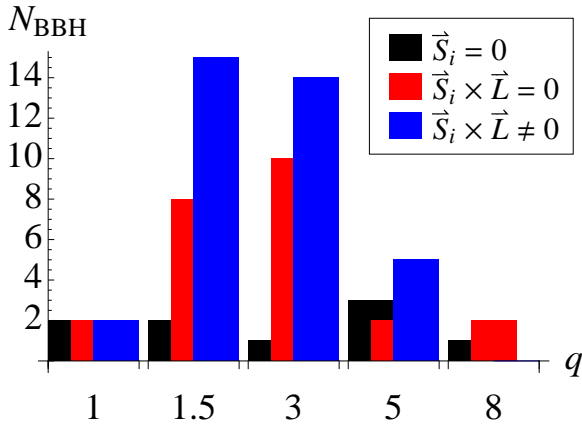


FIG. 3: **Distribution of configurations in set \mathcal{S}_0 .** Given are the number of non-spinning (black), spinning but non-precessing (red) and precessing binaries (blue) for different mass-ratio q .

needed change in orbital frequency and the other the change in radial velocity (or derivative of expansion factor). When plotting parameters during eccentricity removal, Eq. (22) suggests a natural scaling of the axes, relative to the configuration with lowest eccentricity:

$$\delta\Omega_e \equiv 2 \frac{\Omega_0 - \Omega_{0,e=0}}{\Omega_0}, \quad (23)$$

$$\delta\dot{a}_e \equiv \frac{\dot{a}_0 - \dot{a}_{0,e=0}}{\Omega_0}. \quad (24)$$

In these axes, the Euclidean distance to the origin should correspond directly to the eccentricity, cf. Eq. (14). Figure 2 shows the sequence of the eccentricity reduction iterations shown in Fig. 1 plotted in these coordinates. The upper panel of the plot shows $\delta\Omega_e$ and $\delta\dot{a}_e$ as the binary is quasicircularized iteratively. The distance in the $(\delta\dot{a}_e, \delta\Omega_e)$ plane between any point and the origin corresponding to “Iter 4” is equal to the eccentricity e_R . Because Iter 4 is not exactly at zero eccentricity, this distance is only an approximation to Eq. (14), thus explaining the raise of e_Ω/e_R at iterations 2 and 3 in the lower panel of Fig. 2.

C. Binaries in data set \mathcal{S}_0

As a first step, we quasi-circularize iteratively a set of 69 different configurations, which we shall refer to as set \mathcal{S}_0 . The binaries in \mathcal{S}_0 have mass-ratios $1 \leq q \leq 8$. There are 9 non-spinning binaries, 24 spinning binaries with aligned spins (i.e. without precession), and 36 precessing binaries. The dimensionless black hole spin is generally 0.5, but sometimes smaller. The parameters for all 69 configurations are given the first nine columns of Table I in the Appendix, and Fig. 3 show the distribution of non-spinning/aligned spin/non-aligned spins as a function of mass ratio: Most precessing binaries have

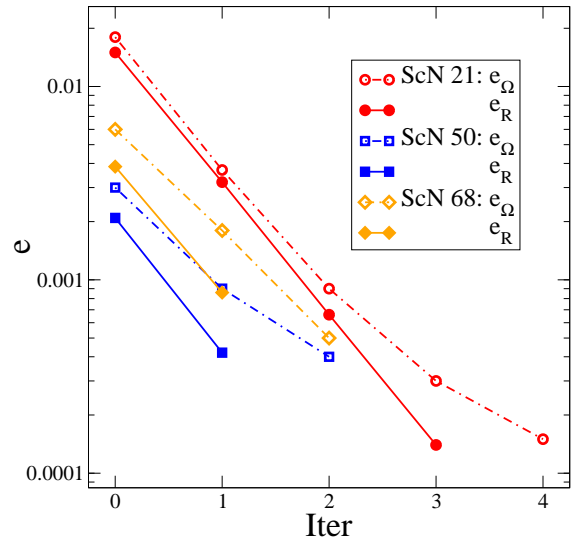


FIG. 4: **Convergence of eccentricity estimates e_Ω and e_R for cases ScN 21, 50 and 68.** Both eccentricity definitions decrease at the same rate to a value below the 10^{-3} limit. The parameters of the three configurations are listed in Table I.

mass ratio either 1.5 or 3. At mass ratio 8, no precessing binaries are evolved.

We apply the iterative eccentricity reduction method to all binaries of set \mathcal{S}_0 . Figure 4 illustrates performance of the iterative eccentricity removal for three cases. This figure compares also the eccentricities e_Ω and e_R . Both eccentricities decrease at the same rate, but the estimated e_R is always smaller than e_Ω , since it is estimated relative to an iteration with finite, albeit small, eccentricity. As we discuss below, e_R is a useful measure to estimate the eccentricity of runs with the same physical parameters but differing orbital parameters Ω_0 and \dot{a}_0 , once the corresponding quasicircularized orbital parameters $\Omega_{0,e=0}$ and $\dot{a}_{0,e=0}$ are known.

Application of iterative eccentricity removal to all binaries in \mathcal{S}_0 results in orbital parameters Ω_0 and \dot{a}_0 as listed in Table I, with an estimated orbital eccentricity e_Ω . Eccentricity removal is terminated once an eccentricity $e_\Omega < 10^{-3}$ is reached except for few runs that are intentionally left with a larger eccentricity for evolutions to compute periastron advance (cf. [40]). The initial and final eccentricities of binaries in set \mathcal{S}_0 are shown in Fig. 5. The red points show the initial eccentricity while the blue point correspond to the final eccentricity.

The initial eccentricities for most of these runs are larger than 0.01. The initial conditions for these runs used PN approximants TaylorT3 to predict the values of the orbital frequency at a given separation, and the radial scaled velocity is set to a small constant value ($\sim -3 \times 10^{-5}$). However, for a few runs, the initial eccentricities are much smaller, almost 10^{-3} . For these simulations, we used Kepler’s law to predict the initial orbital frequency given the quasi-circular parameters of

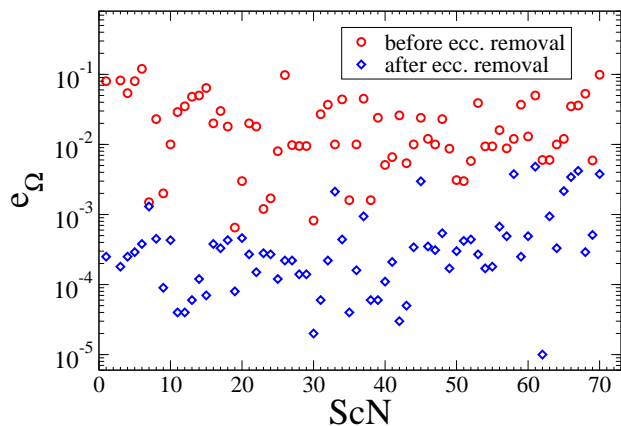


FIG. 5: **Initial and final eccentricities of the configurations in set \mathcal{S}_0 .** The eccentricity reduction target was 10^{-3} , except for runs intentionally left at larger eccentricity for calculations of periastron-advance.

a closely similar configuration. The procedure based on Kepler's law was experimental and motivated the development of more rigorous fitting formulas to predict the initial parameters of quasi-circular binaries, as presented in later parts of this paper.

All quasi-circular binaries in \mathcal{S}_0 were evolved through the inspiral phase until approximately 1–2 orbits before merger. To provide the reader some context about the length of these simulations, Table I lists also the number of evolved orbits up to a orbital frequency $M\Omega = 0.05$. For informational purposes, we also report in Table I the orbital frequency $m\Omega_f$ at which the simple inspiral evolution techniques failed and the number of orbits N_f completed by then. Seven binaries were evolved for more than 30 orbits. The evolutions of merger and ringdown of these binaries require significant extension and refinements of previous spectral merger-techniques [36, 97], and will be reported elsewhere.

D. Binary configurations $\mathcal{S}_1, \dots, \mathcal{S}_5$

As Fig. 5 demonstrates, iterative eccentricity removal by brute force is possible. However, even for some configurations of Fig. 5, the use of ad hoc fitting formulas based on Kepler's law resulted in significantly improved initial guesses Ω_0 and \dot{a}_0 . This allowed to begin iterative eccentricity removal at smaller initial eccentricity, reducing the number of eccentricity-removal iterations and thus lowering the computational cost of iterative eccentricity removal. The goal of this section, therefore, is to construct a much larger sample of low-eccentricity orbital configurations, which will be used in Sec. IV to develop fitting formulae valid for generic BBH systems.

In addition to the 69 configurations of \mathcal{S}_0 , we circularized a total of further 660 configurations, of which 156 are non-precessing (of which 40 are non-spinning) and 504 are precessing. The configurations fall into five sets,

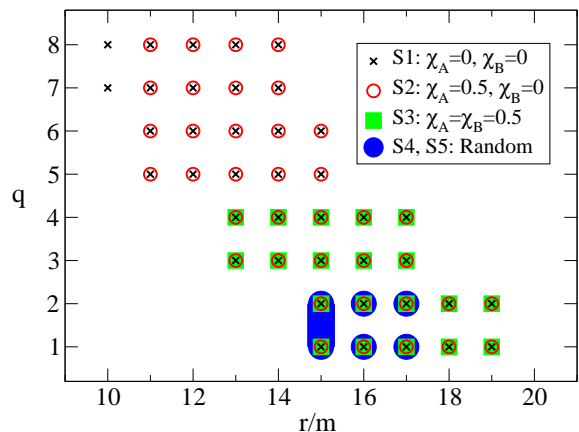


FIG. 6: Parameter space covered with eccentricity removal. Each point in set \mathcal{S}_1 represents one configuration for a total of 40. Each point in set \mathcal{S}_2 represents five different $\vec{\chi}_A$ directions, for a total of 190. Each point in set \mathcal{S}_3 represents 15 different $\vec{\chi}_A$ and $\vec{\chi}_B$ directions, for a total of 300. The set \mathcal{S}_4 and \mathcal{S}_5 contain 130 configurations with randomly generated spin directions and (for 32 of these) randomly generated q .

as indicated in Fig. 6:

- **Set \mathcal{S}_1** contains 40 non-spinning BBH configurations.
- **Set \mathcal{S}_2** contains 190 single-spin configurations where the more massive black hole carries spin $\chi_A = 0.5$. For each $(q, r/m)$ pair, five different spin-directions are considered, with $\theta_A = 0, \pi/4, \pi/2, 3\pi/4, \pi$. The first and the last of these θ_A represent spins aligned and anti-aligned with the orbital angular momentum, so that 76 configurations are non-precessing, while the remaining 114 configurations are precessing.
- **Set \mathcal{S}_3** contains 300 configurations where both black holes carry spin $\chi_A = \chi_B = 0.5$. We consider the same five spin directions for the more massive black hole as in set \mathcal{S}_2 . For each of these, we consider three spin directions for the less massive black hole: $\theta_B = 0, \pi/4, \pi/2$. 40 of the configurations in set \mathcal{S}_3 are non-precessing, and the remaining 260 are precessing.
- **Set \mathcal{S}_4** contains 98 binaries with spin-magnitudes $\chi_A = \chi_B = 0.5$, and random spin-directions. 25 binaries were selected for each combination of mass-ratio $q = 1$ or $q = 2$, and of initial separation $r/m = 16$ or $r/m = 17$. Two of these runs were compromised, so that this results in 98 configurations.
- **Set \mathcal{S}_5** contains 32 binaries with random spin-magnitudes $\chi_{A,B} \leq 0.5$ at random spin-directions with random mass-ratios $q \in [1, 2]$ for fixed $r/m = 15$. The explicit parameters are listed in Table II in the Appendix.

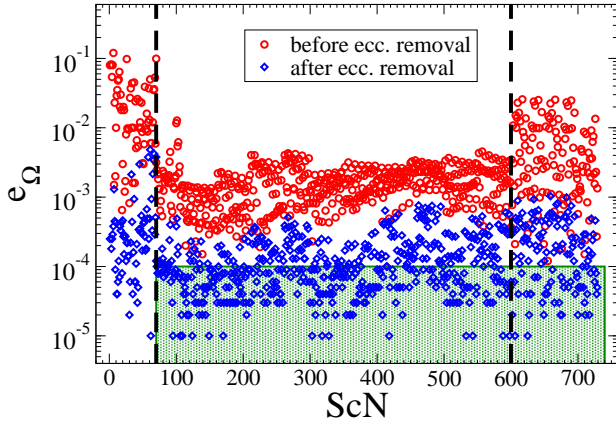


FIG. 7: **Initial and final eccentricities of all runs in the paper.** The first 69 configurations corresponds to the set \mathcal{S}_0 of binaries listed in Table I. The next 530 configurations corresponds to sets $\mathcal{S}_1, \mathcal{S}_2, \mathcal{S}_3$ of binaries, and the last 130 configurations correspond to sets \mathcal{S}_4 and \mathcal{S}_5 with random spin configurations. The final eccentricity of the runs in sets $\mathcal{S}_1, \dots, \mathcal{S}_5$ is reduced to less than 10^{-3} .

Figure 7 summarizes initial and final eccentricity of all configurations which were quasi-circularized. We initialized eccentricity reduction using an ad-hoc formula based on Kepler's law. As can be seen in Fig. 7, this reduced the starting eccentricity of $\mathcal{S}_{1,2,3}$ by about a factor of 10 relative to that of \mathcal{S}_0 . However, it did not significantly reduce the starting eccentricity of the precessing systems in $\mathcal{S}_{4,5}$. A more comprehensive approach is therefore needed.

IV. ECCENTRICITY REDUCTION USING FITTING FORMULAS

Kepler's law helped in quasicircularizing the binaries of the set \mathcal{S}_0 when small variations are introduced in either the separation or the mass ratio of the binary. The Newtonian Kepler's law does not incorporate spin effects in the initial parameters of the binary. Therefore, we will base fitting formulas for spinning binaries on post-Newtonian expansions for spinning binaries.

A. PN formulas

In the post-Newtonian approximations, the initial quasi-circular parameters Ω_0 or \dot{r}_0 (and r_0) are given as a series expansion in m/r (or in Ω_0) for any physical configuration for the binary. We shall use the PN expressions derived by Kidder [98]. In these expressions, non-spinning effects are included up to 2nd post-Newtonian order, while the spin effects enter at 1.5th and 2nd post-Newtonian order. We define the unit vector along the angular momentum $\hat{\mathbf{L}}_{\mathbf{N}} = \mathbf{L}_{\mathbf{N}}/|\mathbf{L}_{\mathbf{N}}|$ where $\mathbf{L}_{\mathbf{N}} \equiv \mu(\mathbf{r} \times \mathbf{v})$ and the spin unit vectors $\hat{\mathbf{s}}_{A,B} = \mathbf{S}_{A/B}/S_{A/B} = \chi_{A/B}/\chi_{A/B}$. Furthermore, let $m = M_A + M_B$ be the total mass, $q = m_A/m_B$ the mass-ratio, $\mu = m_A m_B / m$ be the reduced mass and $\eta \equiv m_A m_B / m^2 = q/(1+q)^2$ the symmetric mass-ratio. In terms of these quantities, Kidder [98] derives the orbital frequency as a function of separation,

$$\begin{aligned} \frac{\Omega^2 r^3}{m} = & 1 - (3 - \eta) \left(\frac{m}{r} \right) - \left[\sum_{i=A,B} \chi_i \hat{\mathbf{L}}_{\mathbf{N}} \cdot \hat{\mathbf{s}}_i \left(2 \frac{m_i^2}{m^2} + 3\eta \right) \right] \left(\frac{m}{r} \right)^{3/2} \\ & + \left[\left(6 + \frac{41}{4} \eta + \eta^2 \right) - \frac{3}{2} \eta \chi_A \chi_B \left(\hat{\mathbf{s}}_{\mathbf{A}} \cdot \hat{\mathbf{s}}_{\mathbf{B}} - 3 \hat{\mathbf{L}}_{\mathbf{N}} \cdot \hat{\mathbf{s}}_{\mathbf{A}} \hat{\mathbf{L}}_{\mathbf{N}} \cdot \hat{\mathbf{s}}_{\mathbf{B}} \right) \right] \left(\frac{m}{r} \right)^2. \end{aligned} \quad (25)$$

The radial velocity as a function of separation is given by:

$$\begin{aligned} \frac{-5}{64} \eta^{-1} \left(\frac{m}{r} \right)^{-3} \dot{r} = & 1 - \frac{1}{336} (1751 + 588\eta) \left(\frac{m}{r} \right) - \left\{ \frac{7}{12} \sum_{i=A,B} \left[\chi_i (\hat{\mathbf{L}}_{\mathbf{N}} \cdot \hat{\mathbf{s}}_i) \left(19 \frac{m_i^2}{m^2} + 15\eta \right) \right] - 4\pi \right\} \left(\frac{m}{r} \right)^{3/2} \\ & - \frac{5}{48} \eta \chi_A \chi_B \left[59 (\hat{\mathbf{s}}_{\mathbf{A}} \cdot \hat{\mathbf{s}}_{\mathbf{B}}) - 173 (\hat{\mathbf{L}}_{\mathbf{N}} \cdot \hat{\mathbf{s}}_{\mathbf{A}}) (\hat{\mathbf{L}}_{\mathbf{N}} \cdot \hat{\mathbf{s}}_{\mathbf{B}}) \right] \left(\frac{m}{r} \right)^2. \end{aligned} \quad (26)$$

The orbital separation r/m as a function of orbital frequency is

$$\begin{aligned} (m\Omega)^{2/3} \frac{r}{m} = & 1 - \frac{1}{3} (3 - \eta) (m\Omega)^{2/3} - \frac{1}{3} \sum_{i=A,B} \left[\chi_i \left(2 \frac{m_i^2}{m^2} + 3\eta \right) \hat{\mathbf{L}}_{\mathbf{N}} \cdot \hat{\mathbf{s}}_i \right] m\Omega \\ & + \left[\eta \left(\frac{19}{4} + \frac{1}{9} \eta \right) - \frac{1}{2} \eta \chi_A \chi_B \left(\hat{\mathbf{s}}_{\mathbf{A}} \cdot \hat{\mathbf{s}}_{\mathbf{B}} - 3 \hat{\mathbf{L}}_{\mathbf{N}} \cdot \hat{\mathbf{s}}_{\mathbf{A}} \hat{\mathbf{L}}_{\mathbf{N}} \cdot \hat{\mathbf{s}}_{\mathbf{B}} \right) \right] (m\Omega)^{4/3}. \end{aligned} \quad (27)$$

And finally, the number of orbits accumulated during inspiral from initial orbital frequency Ω_i to final frequency Ω_f is given by $N = [\Psi(\Omega_i) - \Psi(\Omega_f)] / (2\pi)$ with orbital phase Ψ satisfying

$$32\eta \Psi(\Omega) = (m\Omega)^{-5/3} + \frac{5}{1008}(743 + 924\eta)(m\Omega)^{-1} + \left\{ \frac{5}{24} \sum_{i=A,B} \left[\chi_i \hat{\mathbf{L}}_{\mathbf{N}} \cdot \hat{\mathbf{s}}_i \left(113 \frac{m_i^2}{m^2} + 75\eta \right) \right] - 10\pi \right\} (m\Omega)^{-2/3} \\ + \frac{5}{48} \eta \chi_A \chi_B \left(247 \hat{\mathbf{s}}_{\mathbf{A}} \cdot \hat{\mathbf{s}}_{\mathbf{B}} - 721 \hat{\mathbf{L}}_{\mathbf{N}} \cdot \hat{\mathbf{s}}_{\mathbf{A}} \hat{\mathbf{L}}_{\mathbf{N}} \cdot \hat{\mathbf{s}}_{\mathbf{B}} \right) (m\Omega)^{-1/3}. \quad (28)$$

B. NR Fitting Formulas

The goal of this section is to provide fitting formulae that can predict Ω_0 and \dot{a}_0 as functions of symmetric mass-ratio η , initial black hole spins $\mathbf{S}_{A/B}$ and initial black hole distance r/m . This is an 8-dimensional parameter space. As we shall see, linear fits are not sufficient, however, if one were to write a straightforward 8-dimensional higher-order Taylor-series, the number of coefficients would quickly explode with expansion order. Therefore, one needs to be judicious to include only terms that contribute to the fit.

Motivated by Eqs. (25) and (26), we do *not* write down fitting formulae directly for Ω_0 and \dot{a}_0 , but rather for the quantities

$$\kappa_0 \equiv \frac{\Omega_0^2 r_0^3}{m} \quad (29)$$

and

$$\rho_0 \equiv -\frac{5m}{64\eta} \left(\frac{r_0}{m} \right)^4 \dot{a}_0. \quad (30)$$

For each quasi-circular configuration, we compute κ_0 and ρ_0 .

Beginning to fit the non-spinning components, we only consider the quasi-circular configurations of set \mathcal{S}_1 and fit polynomials in η and inverse distance $u \equiv m/r$:

$$\kappa_{\text{NS}} = \sum_{i,j=0}^{i+j \leq 3} b_{i,j} \eta^i u^j, \quad (31)$$

$$\rho_{\text{NS}} = \sum_{i,j=0}^{i+j \leq 3} a_{i,j} \eta^i u^j. \quad (32)$$

(Here, the subscript 'NS' refers to non-spinning binaries). We found that the triangular truncation $i + j \leq 3$ gave a good fit with a reasonably low number of coefficients. The coefficients $a_{i,j}$ and $b_{i,j}$ are listed in Tables III and IV.

For spinning binaries of sets \mathcal{S}_2 , \mathcal{S}_3 , \mathcal{S}_4 and \mathcal{S}_5 , we first subtract the fits Eqs. (31) and (32), i.e. we compute for each spinning quasi-circular configuration

$$\delta\kappa_S \equiv \kappa_0 - \kappa_{\text{NS}}|_{\eta_0, u_0}, \quad (33)$$

$$\delta\rho_S \equiv \rho_0 - \rho_{\text{NS}}|_{\eta_0, u_0}. \quad (34)$$

The functions $\delta\kappa_S$ and $\delta\rho_S$ should be functions of the spins of the black holes, mass-ratio and separation. These functions should vanish for zero spins, to reduce to the fit for non-spinning BBH.

We will use in total 14 basis-functions to represent the spin-sector, which we shall label \hat{e}_α , $\alpha = 1, \dots, 14$. The first four basis-functions take the functional form of the spin-terms in Eqs. (25)–(28):

$$\hat{e}_1 = \mathbf{S}_A \cdot \hat{\mathbf{L}}, \quad (35a)$$

$$\hat{e}_2 = \mathbf{S}_B \cdot \hat{\mathbf{L}}, \quad (35b)$$

$$\hat{e}_3 = \mathbf{S}_A \cdot \mathbf{S}_B, \quad (35c)$$

$$\hat{e}_4 = \mathbf{S}_{A,\perp} \cdot \mathbf{S}_{B,\perp}, \quad (35d)$$

where $\mathbf{S}_{i,\perp} = \mathbf{S}_i - \hat{\mathbf{L}}(\hat{\mathbf{L}} \cdot \mathbf{S}_i)$, $i = A, B$ are the projections of each black hole spin into the orbital plane.

The next two basis-functions account for the angle between $\mathbf{S}_{A/B}$ relative to the other black hole:

$$\hat{e}_5 = \mathbf{S}_A \cdot \hat{\mathbf{r}}, \quad (35e)$$

$$\hat{e}_6 = \mathbf{S}_B \cdot \hat{\mathbf{r}}, \quad (35f)$$

where $\hat{\mathbf{r}}$ is the unit-vector pointing from black hole 2 to black hole 1. These terms are not present in the post-Newtonian expansion. However, we find them to be necessary for a good fit. We conjecture that the origin of these terms rests in details of how numerical BBH initial data is constructed. For instance, conformally flat quasi-equilibrium BBH initial data requires a somewhat different choice of \dot{a}_0 to achieve low eccentricity compared to superposed Kerr-Schild data [99, 100]. Both types of initial-data require some offset in \dot{a}_0 relative to post-Newtonian expansions, and the need to include \hat{e}_5 and \hat{e}_6 when fitting for low-eccentricity initial data parameters indicates that this offset depends on the angle between black hole spin and direction to the partner black hole.

Finally, as demonstrated below, the fit of the spin-sector can be improved by including certain higher-order

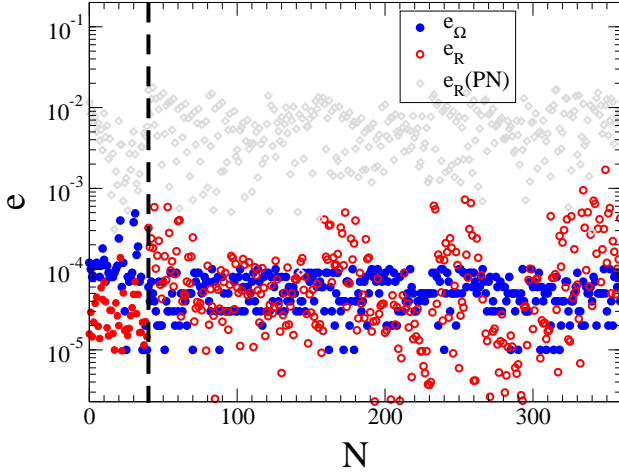


FIG. 8: Eccentricities e_Ω and e_R for the binaries of the sets \mathcal{S}_2 , and those configurations of $\mathcal{S}_{3,4,5}$ with $e_\Omega \leq 0.0001$. The residuals e_R of the fitting formulas are comparable to the actual estimated eccentricity e_Ω . Further, improvement of the fitting formulas requires quasi-circular configuration with lower eccentricities e_Ω . The first 40 simulations are nonspinning. The expected PN eccentricities are plotted in grey.

basis-functions:

$$\hat{e}_7 = (\mathbf{S}_A \cdot \hat{\mathbf{L}})^2, \quad (35g)$$

$$\hat{e}_8 = (\mathbf{S}_A \cdot \hat{\mathbf{L}})^3, \quad (35h)$$

$$\hat{e}_9 = (\mathbf{S}_B \cdot \hat{\mathbf{L}})^2, \quad (35i)$$

$$\hat{e}_{10} = (\mathbf{S}_B \cdot \hat{\mathbf{L}})^3, \quad (35j)$$

$$\hat{e}_{11} = (\mathbf{S}_A \cdot \mathbf{S}_B)^2, \quad (35k)$$

$$\hat{e}_{12} = (\mathbf{S}_{A,\perp} \cdot \mathbf{S}_{B,\perp})^2, \quad (35l)$$

$$\hat{e}_{13} = (\mathbf{S}_A \cdot \hat{\mathbf{r}})^2, \quad (35m)$$

$$\hat{e}_{14} = (\mathbf{S}_B \cdot \hat{\mathbf{r}})^2. \quad (35n)$$

The functions $\delta\kappa_S$ and $\delta\rho_S$ are expanded into a series that depends on η , u and the spin basis \hat{e}_α :

$$\delta\kappa_S = \sum_{i=0}^3 \sum_{j=2}^5 \sum_{\alpha=1}^{14} c_{i,j,\alpha} \eta^i u^{j/2} \hat{e}_\alpha, \quad (36)$$

$$\delta\rho_S = \sum_{i=0}^3 \sum_{j=2}^5 \sum_{\alpha=1}^{14} d_{i,j,\alpha} \eta^i u^{j/2} \hat{e}_\alpha. \quad (37)$$

These expansions have 224 coefficients each. For our best result, we fit these coefficients against that subset of configurations of the sets $\mathcal{S}_{3,4,5}$ which have $e_\Omega < 10^{-4}$. These configurations are located in the green shaded region of Fig. 7. The resulting coefficients are listed in Tables V and VI in the Appendix.

C. Quality of the fitting formulas

The quasi-circular orbital parameters that form the basis of the fits Eqs. (36) and (37) are not perfectly accu-

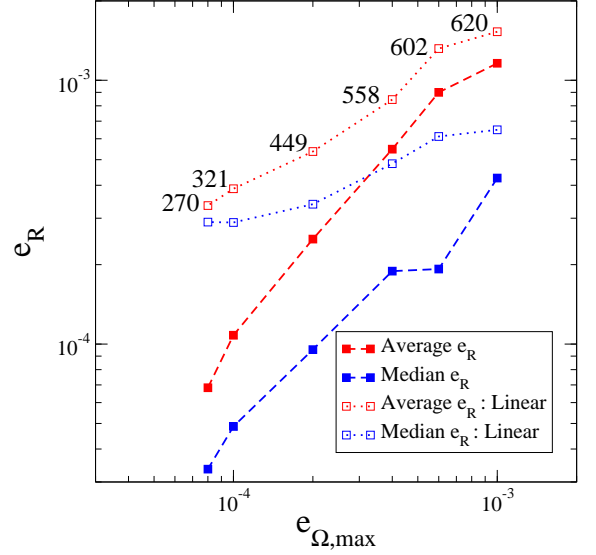


FIG. 9: **Performance of fit vs. the eccentricity of the configurations used in the fit.** Eccentricity fits are performed only using those configurations with $e_\Omega < e_{\Omega,\max}$. As a function of $e_{\Omega,\max}$ the plot shows the average and the median of e_R . Reducing the eccentricity $e_{\Omega,\max}$ improves the fitting formulas performance. The numbers indicate the number of configurations used in each fit.

rate; rather they contains residual eccentricity as indicated in Fig. 7. Therefore, we should expect the low-eccentricity fits to be good to only a comparable level of precision. If the fits were more accurate than indicated by Fig. 7, this would indicate a fit to the *errors* in the numerical data, which would not carry any additional physical information. To quantify the quality of the fits, we translate the residuals

$$\Delta\Omega_0 = \Omega_{0,\text{NR}} - \Omega_{0,\text{fit}}, \quad (38)$$

$$\Delta\dot{a}_0 = \dot{a}_{0,\text{NR}} - \dot{a}_{0,\text{fit}} \quad (39)$$

into an equivalent eccentricity via Eq. (15):

$$e_R = \left[\left(\frac{\Delta\dot{a}_0}{\Omega_{0,\text{NR}}} \right)^2 + \left(\frac{\Delta\Omega_0}{\Omega_{0,\text{NR}}} \right)^2 \right]^{1/2}. \quad (40)$$

Our target is that e_R as computed from the fits is roughly comparable to the eccentricity e_Ω of the data used to compute the fits. If $e_R \gg e_\Omega$ the fit is not as accurate as it could be; if $e_R \ll e_\Omega$, the fit has so many degrees of freedom that it fits the residual eccentricity of the NR simulations. Figure 8 demonstrates that indeed $e_R \sim e_\Omega$, as desired.

The dependence of the quality of the fit onto the configurations used for the fit is further explored in Fig. 9. For this figure, we perform the fit for the spinning sector $\delta\kappa_S$, $\delta\rho_S$ several times, based on those configurations within $\mathcal{S}_{3,4,5}$ with eccentricity $e_\Omega \leq e_{\Omega,\max}$. The dashed curves of Fig. 9 show the residual eccentricity e_R of these fits as a function of threshold eccentricity $e_{\Omega,\max}$. For the

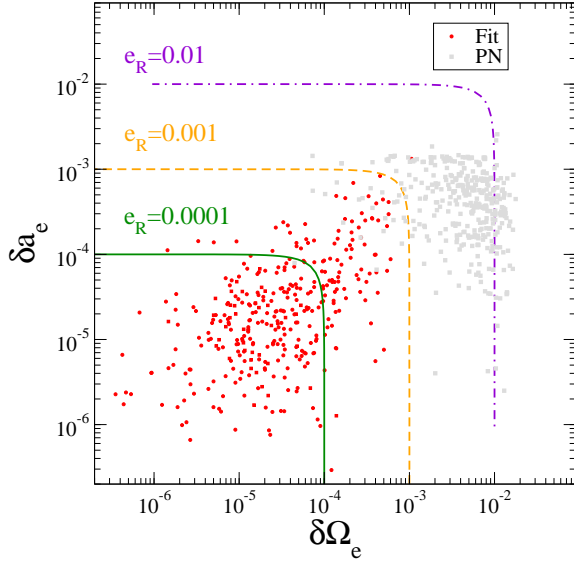


FIG. 10: **Eccentricities** ($\delta a_e, \delta \Omega_e$) **for the binaries of the sets** $\mathcal{S}_1, \dots, \mathcal{S}_5$ **with** $e \leq 0.0001$ **as predicted by the the fitting formulas and the PN expressions.** Most binaries have an eccentricity less than 0.0001 when using the fitting formulas, while PN expressions generate binaries with nearly 0.01 eccentricity. The fits yield lower eccentricity than PN expansions, with the improvement primarily due to the more accurate prediction of radial velocity (δa_e). We plot the fits based on binaries with eccentricity less than 0.0001.

dashed lines the residual of the fit e_R is similar to $e_{\Omega, \max}$, indicating that the fit works as well as can be expected. If the basis-functions for the spin-sector are restricted to only the linear terms, $\hat{e}_\alpha, \alpha = 1, \dots, 6$, then we obtain the dotted lines. Now the residual eccentricity is several times larger than $e_{\Omega, \max}$, indicating the possibility to improve the fit.

We now compare our low-eccentricity fits with post-Newtonian expansions that predict initial data parameters. Using Eqns. (25) and (26) we compute Ω_{PN} and \dot{a}_{PN} for each configuration. We then compute the difference between eccentricity-reduced NR parameters and the PN parameters,

$$\delta \Omega_e \equiv 2 \frac{\Omega_{0, \text{PN}} - \Omega_{0, \text{NR}}}{\Omega_{0, \text{NR}}}, \quad (41)$$

$$\delta \dot{a}_e \equiv \frac{\dot{a}_{0, \text{PN}} - \dot{a}_{0, \text{NR}}}{\Omega_{0, \text{NR}}}, \quad (42)$$

$$e_{R, \text{PN}} \equiv \sqrt{\delta \Omega_e^2 + \delta \dot{a}_e^2}. \quad (43)$$

Because we know low-eccentricity orbital parameters $\Omega_{0, \text{NR}}, \dot{a}_{0, \text{NR}}$ these formulae allow us to estimate the eccentricity the PN parameters would have *without* having to evolve with the PN initial-data parameters. Figure 8 shows this estimated eccentricity $e_{R, \text{PN}}$ as the grey dots. Our fits improve the post-Newtonian initial data parameters by about two orders of magnitude, consistently for all spin-directions, including precessing binaries.

Figure 10 plots separately the two components $\delta \Omega_e$ and $\delta \dot{a}_e$, cf. Eqs. (41) and (42). The plot shows the PN data in grey and the results of the fitting formulas as red circles. Once again, the improvement gained by the fits is apparent: The eccentricity is smaller by nearly two order of magnitude relative to PN initial-data parameters. We also note that for the fit, $\delta \dot{a}_e$ and $\delta \Omega_e$ have approximately equal magnitudes. For PN, in contrast, $\delta \Omega_e$ is about a factor ~ 10 larger than $\delta \dot{a}_e$, indicating that an error in the orbital frequency is the major cause of eccentricity when using PN parameters.

D. Number of orbits fits

When selecting initial data parameters for an evolution, it is useful to be able to estimate of how long the simulation will be. One widely used measure is the number of orbits the binary completes before merger. We have evolved the binaries in sets \mathcal{S}_0 and \mathcal{S}_5 through inspiral phase, so we can use this information to derive a fitting formula for the number of orbits. We base this fitting formula on Eqs. (28), specifically

$$N = \frac{1}{2\pi} (\Psi_{\text{fit}}(\Omega_i) - \Psi_{\text{fit}}(\Omega_f)). \quad (44)$$

The fitting parameters d_1, \dots, d_9 are incorporated into the phase-formula,

$$\begin{aligned} 32\eta \Psi_{\text{fit}}(\Omega) = & (m\Omega)^{-5/3} + \frac{5(743d_1 + 924d_2\eta)}{1008} (m\Omega)^{-1} + \left\{ \sum_i \left[\frac{5\chi_i}{24} \hat{\mathbf{L}}_{\mathbf{N}} \cdot \hat{\mathbf{s}}_i \left(113d_7 \frac{m_i^2}{m^2} + 75d_8\eta \right) \right] - 10\pi d_3 \right\} (m\Omega)^{-2/3} \\ & + \left[(d_4 + d_5\eta + d_6\eta^2) + \frac{5}{48} d_9 \eta \chi_A \chi_B \left(247\hat{\mathbf{s}}_{\mathbf{A}} \cdot \hat{\mathbf{s}}_{\mathbf{B}} - 721\hat{\mathbf{L}}_{\mathbf{N}} \cdot \hat{\mathbf{s}}_{\mathbf{A}} \hat{\mathbf{L}}_{\mathbf{N}} \cdot \hat{\mathbf{s}}_{\mathbf{B}} \right) \right] (m\Omega)^{-1/3}. \end{aligned} \quad (45)$$

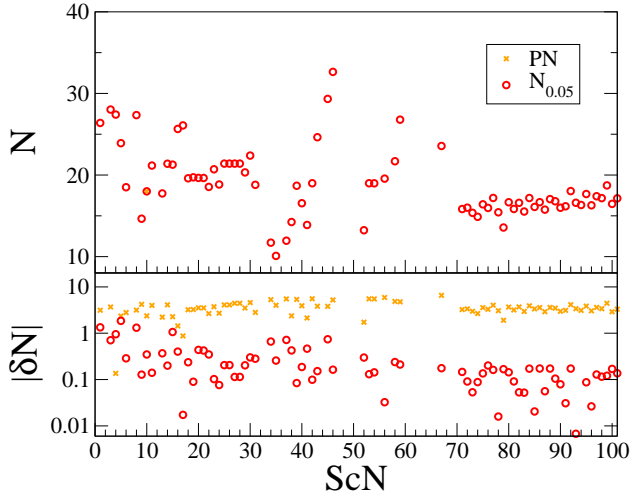


FIG. 11: **The number of orbits of the runs and the residual of the fitting formulas.** In the upper panel, we plot the number of orbits $N_{0.05}$ through the inspiral in red between the initial orbital frequency Ω_i and the final orbital frequency $\Omega = 0.05/m$ evolved. In the lower panel, we plot the difference between the fitting polynomial and the numerical data of the number of orbits in red. We compare the results to the PN approximation plotted in orange.

The number of orbits is fitted to Eqs. (44) and (45) using the inspiral data from sets \mathcal{S}_0 and \mathcal{S}_5 as given in Tables I and II. We include only those inspirals that reach orbital frequency $0.05/m$ or greater, that inspiral for at least 10 orbits and that have an eccentricity of less than 0.005.

The results of the fit for N are shown in Fig. 11. The upper panel of Fig. 11 plot the number of orbits evolved between the initial orbital frequency Ω_i and the final orbital frequency $0.05/m$ for the inspirals used in these fits. For the first 69 simulations of set \mathcal{S}_0 , binaries with large differences in the initial separation and mass ratios are evolved. Therefore, a large variation in the number of orbits is observed. For the last 32 runs of set \mathcal{S}_5 , all binaries start with the same initial separation but with a random mass ratio and spin orientation and magnitude. In this case, their number of orbits varies between 15 and 20.

In the lower panel of Fig. 11, we plot the difference between the number of orbits measured up to a certain orbital frequency, and the number predicted by the fitting formula (44) as red points. This residual is less than 1 orbit for the set \mathcal{S}_0 , and it is less than 0.2 orbits for the binaries of set \mathcal{S}_5 . No variation in the quality of the fits is noticed as we changed the final frequency from $0.05/m$. We use also the PN expression in Eq. 28 to plot the difference in the number of orbits between the numerical simulations and the PN predictions measured at an orbital frequency of $0.05/m$ in orange. The initial frequency used is the value for which the simulation starts with, i.e. Ω_i . The straight post-Newtonian formula predicts a number of orbits that generally differs by 3 to 6

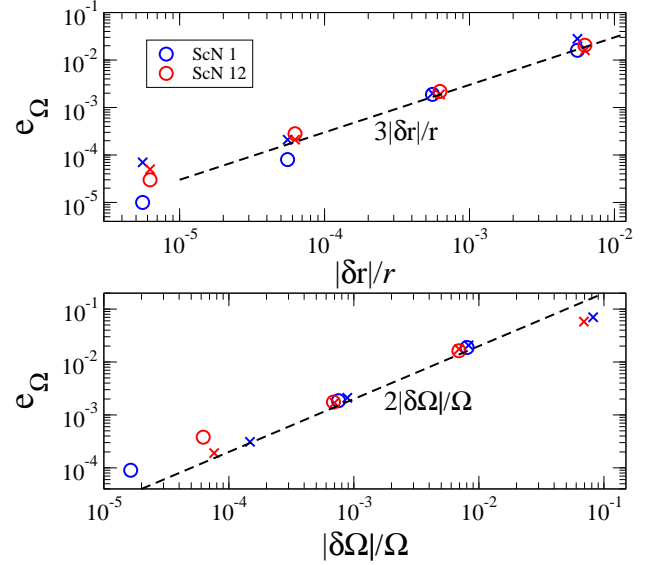


FIG. 12: Eccentricity of runs with initial data parameters perturbed from their low-eccentricity values. Two representative configurations are shown, ScN 1 (equal mass, zero spin), and ScN 12 ($q=1.5$, precessing spin). Circles are for positive variations, while crosses are for negative variation. The dashed line represents the expectation, Eq. (14).

orbits from the NR result.

V. GENERATING INITIAL DATA WITH A PRE-DETERMINED ECCENTRICITY

So far, we have been concerned with achieving BH-BH simulations with very small eccentricity. Let us now consider how to choose initial-data parameters that result in some desired *non-zero* eccentricity. If one starts from known zero-eccentricity orbital parameters $(r_0, \Omega_0, \dot{a}_0)$, and perturbs these, $(r_0 + \delta r, \Omega_0 + \delta \Omega, \dot{a}_0 + \delta \dot{a})$, then the Newtonian formula Eq. (14) should give a reasonable approximation of the resulting eccentricity. To test this assumption we use two eccentricity-removed configurations, ScN 1 (equal mass, zero spin) and ScN 12 (mass-ratio 1.5, precessing). We perturb first by changing the initial separation while keeping Ω_0 and \dot{a}_0 constant, and, second, by changing Ω_0 while keeping d_0 and \dot{a}_0 constant. For each perturbation, we solve for a new initial-data set, and evolve long enough to measure e_Ω . The results are plotted in Fig. 12, along with the result of Eq. (14), $e = 3|\delta r|/r$ and $e = 2|\delta \Omega|/\Omega$, respectively.

The agreement between the full numerical simulation and the Newtonian formula is very good. The exceptions are very low eccentricity $e_\Omega \lesssim 10^{-4}$, where measuring eccentricity in the numerical simulation is difficult, and for very large eccentricity $e \sim 0.1$, where linear perturbations may no longer be adequate. Besides controlling eccentricity, one can also use Eq. (16) to control the phase or periastron.

So far, we have perturbed off a zero-eccentricity configuration. As we have seen in Sec. III, our fitting formulae for initial data-parameters result in eccentricities $e \lesssim 10^{-3}$. If one is interested in eccentricities larger than this value, then one can also perturb around the results of the low-eccentricity fitting formulas. This now allows to obtain a BH-BH simulation with desired length (via Eq. 28) and desired eccentricity, via the fitting formulas for low-eccentricity parameters and Eq. (14) and (16), *without* any iterative procedures.

VI. CONCLUSIONS

Evolutions of binary black holes start from initial data. Choices that enter the initial data determine the orbital eccentricity of the subsequent evolution, and the length of the inspiral (i.e. the number of orbits to merger). This paper presents techniques that allow to choose initial data parameters that result in very small eccentricity ($e \sim 10^{-4}$) with an inspiral of a desired number of orbits. We also present techniques that allow to choose initial data parameters that result in a desired non-zero eccentricity. Our techniques are applicable for *generic* precessing binary black holes of mass-ratios $q \lesssim 8$ and for spin-magnitudes $\lesssim 0.5$. Because of fitting formulae we develop here, the use of these techniques requires no significant computational cost.

This paper presents quasi-circular initial data for 729 different configurations (mass-ratio, separation, spins) of binary black holes. This study covers for the first time a full 7-dimensional *voluminous* region of parameter space of generic non-eccentric BBH inspirals, rather than just lower-dimensional subspaces like aligned spin binaries (e.g. [17]). The mass ratio varies between 1 and 8 for these simulations, 620 binaries are spinning, most of these with generic, precessing spins of dimensionless magnitude up to 0.5.

The orbital eccentricity of all 729 configurations is iteratively reduced using techniques developed in earlier work [54, 66, 67]. To remove or ease the computational burden of iterative eccentricity removal, we introduce fitting formulas that predict low-eccentricity orbital parameters. Fitting the 2-dimensional non-spinning sector spanning mass-ratio and spin requires 10 fitting parameters each in the formulae for orbital frequency and radial velocity. Extending this fit to the 8-dimensional spinning-sector (mass-ratio, separation, two spin vectors) required 224 fitting parameters each. Perhaps surprisingly, despite the comparatively low spins considered here $\chi \lesssim 0.5$, higher order corrections to the spin incorporated via Eqs. (35g)–(35n) noticeably improve the quality of the fit, cf. Fig. 9. We also provide a fitting formula for the expected number of orbits during the inspiral of low-eccentricity initial data, again for generic precessing spins and mass-ratios.

The fitting formulas allow to achieve BH-BH configurations of desired initial separation (or desired initial

orbital frequency or desired number of orbits) with an eccentricity of $\sim 10^{-4}$ without having to perform any iterative runs. If lower eccentricity is desired, it is always possible to refine by iterative eccentricity removal.

Based on these fits, we develop a technique to predict the eccentricity of initial-data parameters without having to evolve the initial data at all. This technique is based on the deviation of the initial-data parameters from those for low-eccentricity (the latter determined either from our bank of 729 configurations, or computed from our low-eccentricity fits), cf. Eqs. (41)–(43). It allows us to estimate the orbital eccentricity that would have resulted from post-Newtonian initial data parameters without constructing initial data for those configurations. The results are shown in Figs. 8 and 10 demonstrating that our fitting formulas yield orbital eccentricity about two orders of magnitude smaller than post-Newtonian expansions.

The ability to estimate eccentricity without an evolution is also useful in another scenario: To obtain an evolution with desired eccentricity, one can simply perturb the low-eccentricity fits and use Eqs. (41)–(43) to determine the eccentricity of the perturbed initial-data. This procedure allows to construct initial data of desired eccentricity without having to perform any intermediate evolutions. This procedure is demonstrated in Sec. V.

During the construction of BBH initial-data, free parameters like initial orbital frequency and initial radial velocity must be chosen. Early in the evolution, the space-time relaxes to a quasi-stationary steady state, changing the black hole parameters slightly and emitting a pulse of “junk radiation” [101]. This relaxation causes orbital frequency and radial velocity (and also black hole masses and spins, albeit to a smaller degree [30]) to deviate from the corresponding parameters specified in the initial-data. These drifts depend on the precise type of initial data evolved (e.g. conformally flat conformal-thin sandwich data, as here; super-posed Kerr-Schild data; puncture data) and may exhibit a dependence on black hole parameters *different* from the usual post-Newtonian terms. These drifts in parameters, induced by specific choices of the initial-data construction, may very well be the reason why our fitting formulas require terms that are not present in post-Newtonian expansions, cf. Eqs. (31) and (32). Because these drifts—as well as the coordinate systems used when constructing initial data—are different for each class of initial-data, we expect that a similar fitting effort is necessary for superposed Kerr-Schild data, which allows access to higher black-hole spins.

Out of the 729 configurations, we evolve 101 simulations fully through inspiral. Only the number of orbits of each inspiral was used here in order to write fitting formulas for any spinning configurations. Because of the wealth of information in these simulations, they will form the basis of a large number of future investigations into periastron-advance, black hole remnant properties, analytic template modelling, and gravitational wave data-analysis efforts.

Acknowledgments

We would like to thank Mike Boyle, Tony Chu, Larry Kidder, Geoffrey Lovelace, Mark Scheel, Bela Szilagyi and Nick Taylor for useful discussions. We gratefully acknowledge support from the NSERC of Canada, from the Canada Research Chairs Program, and from the Canadian Institute for Advanced Research. Computations

were performed on the GPC supercomputer at the SciNet HPC Consortium. SciNet is funded by: the Canada Foundation for Innovation under the auspices of Compute Canada; the Government of Ontario; Ontario Research Fund - Research Excellence; and the University of Toronto. Results obtained in this paper were produced using the Spectral Einstein Code (SpEC) [78].

Appendix: Tables

TABLE I: **Parameters of the runs evolved in S_0 .** The first column is the label for each configuration (we refer to individual runs as “Sc21”), the following columns show the mass ratio q , the separation r/m , the initial orbital frequency Ω_i , the dimensionless expansion factor \dot{a} , the spin components of the first hole χ_A and the spin of the second hole χ_B , the eccentricity e_Ω , the final orbital frequency Ω_f , the number of orbits N_f between the initial frequency Ω_i and the final frequency Ω_f . The last column denotes the number of orbits between the initial orbital frequency until the orbital frequency $0.05/m$.

ScN	q	r/m	χ_A	θ_A/π	ϕ_A/π	χ_B	θ_B/π	ϕ_B/π	$10^2 m \Omega_i$	$10^5 \dot{a}$	$10^4 e_\Omega$	$10^2 m \Omega_f$	N_f	$N_{0.05}$
1	1	18	0	0	0	0	0	0	1.2202	-2.54	2.5	12.	27.9	26.38
2	1	19	0	0	0	0	0	0	1.1292	-2.10	1.8	3.3	28.4	-
3	1	18	0.5	0	0	0	0	0	1.2168	-1.63	2.5	7.5	29.2	28.02
4	1	19	0.5	0.5	0	0	0	0	1.1283	-1.88	2.9	8.0	31.7	27.41
5	1	19	0.5	1	0	0	0	0	1.1313	-2.80	3.8	4.2	28.1	23.90
6	1.345	16	0.320	0.667	0.142	0.150	0.732	0.148	1.4463	-3.60	2.4	12.	19.94	18.50
7	1.5	16	0	0	0	0	0	0	1.4427	-3.64	13.0	13.	21.1	19.50
8	1.5	18	0	0	0	0	0	0	1.2199	-2.15	4.5	13.	28.9	27.34
9	1.5	14	0.5	0	0	0	0	0	1.7367	-5.14	0.9	6.3	15.5	14.65
10	1.5	16	0.5	0.833	0	0	0	0	1.4481	-5.11	4.3	7.5391	18.8	18.00
11	1.5	16	0.5	0.167	0	0	0	0	1.4384	-2.94	0.4	7.6682	22.4	21.16
12	1.5	16	0.5	0.5	0	0	0	0	1.4427	-3.64	0.4	9.8	20.9	-
13	1.5	16	0.5	1	0	0	0	0	1.4490	-4.76	0.6	7.5	18.5	17.74
14	1.5	16	0.5	0	0	0	0	0	1.4379	-2.72	1.2	7.1	22.5	21.38
15	1.5	17	0.5	1	0	0	0	0	1.3286	-3.82	0.7	7.7	22.0	21.27
16	1.5	18	0.5	0.5	0	0	0	0	1.2192	-2.11	3.3	9.4	28.9	25.65
17	1.5	19	0.5	1	0	0	0	0	1.1321	-2.26	4.3	7.6	30.3	26.08
18	1.5	16	0.5	0.5	0	0.5	0.5	1	1.4424	-3.31	0.8	5.6	20.0	19.60
19	1.5	16	0.5	0.5	0	0.5	0.5	0	1.4414	-3.34	4.6	5.5	20.1	19.72
20	1.5	16	0.5	0.5	0	0.5	0.5	-0.5	1.4534	-3.60	2.7	6.8	20.5	19.65
21	1.5	16	0.5	0.5	0	0.5	0.5	0.5	1.4533	-3.61	1.5	7.8	20.7	19.64
22	1.5	16	0.5	0.5	0	0.5	1	0	1.4455	-5.02	2.8	5.7	18.9	18.54
23	1.5	16	0.5	0.5	0	0.5	0	0	1.4388	-2.62	2.7	6.6	21.6	20.70
24	1.5	16	0.5	1	0	0.5	0	0	1.4446	-3.48	1.2	7.3	19.7	18.84
25	1.5	16	0.5	0	0	0.5	0.5	1	1.4370	-2.74	2.2	6.8	22.4	21.40
26	1.5	16	0.5	0	0	0.5	0.5	0	1.4370	-2.74	2.2	6.8	22.4	21.40
27	1.5	16	0.5	0	0	0.5	0.5	-0.5	1.4485	-2.57	1.4	5.5	21.8	21.40
28	1.5	16	0.5	0	0	0.5	0.5	0.5	1.4485	-2.57	1.4	5.5	21.8	21.40
29	1.5	16	0.5	0	0	0.5	1	0	1.4402	-3.93	0.2	6.8	21.2	20.32
30	1.5	16	0.5	0	0	0.5	0	0	1.4344	-1.56	0.6	7.1	23.72	22.38
31	1.5	16	0.320	0.667	0.142	0.150	0.732	0.148	1.4463	-3.60	2.2	11.	20.2	18.80
32	3	14	0	0	0	0	0	0	1.7427	-4.69	21.2	8.3	17.6	16.36
33	3	12	0.5	0.833	0	0	0	0	2.1817	-11.5	4.4	8.3	9.3	8.36
34	3	12	0.5	0.167	0	0	0	0	2.1522	-7.72	0.4	9.2	13.7	11.71
35	3	12	0.5	0.5	0	0	0	0	2.1644	-8.89	1.6	7.9	11.4	10.09
36	3	12	0.5	1	0	0	0	0	2.1846	-12.3	9.4	10.	9.1	8.08
37	3	12	0.5	0	0	0	0	0	2.1508	-7.74	0.6	9.3	14.1	11.95
38	3	14	0.5	0.833	0	0	0	0	1.7538	-5.91	0.6	9.6	15.3	14.24
39	3	14	0.5	0.167	0	0	0	0	1.7348	-4.24	1.1	8.8	20.6	18.69
40	3	14	0.5	0.5	0	0	0	0	1.7427	-4.69	2.1	9.6	18.1	16.54

Continued

TABLE I – *Continued*

ScN	q	r/m	χ_A	θ_A/π	ϕ_A/π	χ_B	θ_B/π	ϕ_B/π	$10^2 m\Omega_i$	$10^5 \dot{a}$	$10^4 e_\Omega$	$10^2 m\Omega_f$	N_f	$N_{0.05}$
41	3	14	0.5	1	0	0	0	0	1.7559	-6.15	0.3	9.9	14.9	13.88
42	3	14	0.5	0	0	0	0	0	1.7338	-3.95	0.5	8.7	21.0	18.99
43	3	16	0.5	0.5	0	0	0	0	1.4420	-2.83	3.4	10.	26.1	24.63
44	3	16	0.5	1	0	0	0	0	1.4494	-4.70	29.8	10.	22.1	21.13
45	3	17	0.5	0.5	0	0	0	0	1.3227	-2.43	3.5	8.5	30.7	29.33
46	3	17	0.5	0	0	0	0	0	1.3175	-2.00	3.1	6.1	33.8	32.64
47	3	18	0.5	1	0	0	0	0	1.2251	-2.06	5.4	9.1	31.4	24.98
48	3	14	0.5	0.5	0	0.5	0.5	1	1.7423	-4.18	1.7	2.7	11.4	-
49	3	14	0.5	0.5	0	0.5	0.5	0	1.7409	-4.27	3.0	2.7	11.4	-
50	3	14	0.5	0.5	0	0.5	1	0	1.7445	-5.78	4.2	2.8	11.7	-
51	3	14	0.5	0.5	0	0.5	0	0	1.7391	-3.23	4.4	2.6	11.1	-
52	3	14	0.5	1	0	0.5	1	0	1.7583	-7.93	2.7	5.9	13.6	13.23
53	3	14	0.5	0	0	0.5	0.5	1	1.7325	-3.86	1.7	5.6	19.6	18.99
54	3	14	0.5	0	0	0.5	0.5	0	1.7324	-3.73	1.8	5.6	19.6	18.98
55	3	14	0.5	0	0	0.5	1	0	1.7346	-6.27	6.7	7.7	19.9	18.34
56	3	14	0.5	0	0	0.5	0	0	1.7302	-2.86	4.9	5.3	19.9	19.56
57	5	12	0	0	0	0	0	0	2.1686	-5.96	37.7	9.1	14.9	13.32
58	5	14	0	0	0	0	0	0	1.7433	-3.50	2.5	9.7	23.4	21.69
59	5	15	0	0	0	0	0	0	1.5809	-2.84	4.9	8.3	28.3	26.78
60	5	9.5	0.323	0.663	-0.176	0	0	0	3.0132	-19.9	48.2	5.9	5.6	4.99
61	5	9.5	0.483	0.642	-0.212	0	0	0	3.0132	-19.9	0.1	8.5	4.7	4.73
62	5	9.5	0.5	0.644	-0.213	0	0	0	3.0132	-19.9	9.4	4.5	4.2	4.26
63	5	12	0.5	0.644	-0.213	0	0	0	2.1755	-9.02	3.3	2.0	7.8	7.75
64	5	15	0.5	0.5	0	0	0	0	1.5787	-2.87	21.6	2.1	13.5	-
65	5	15	0.5	1	0	0	0	0	1.5906	-4.38	34.2	9.4	22.9	21.97
66	5	15	0.5	0	0	0	0	0	1.5695	1.62	42.0	5.6	31.7	30.93
67	8	13	0	0	0	0	0	0	1.9345	-2.98	2.9	6.8	24.9	23.56
68	8	13	0.5	1	0	0	0	0	1.9536	-4.21	5.1	7.0	18.7	17.99
69	8	13	0.5	0	0	0	0	0	1.9221	-4.76	37.8	6.4	31.7	29.41

TABLE II: **Parameters of the runs evolved in S_5 .** The first column labels the binary configuration, $q = m_A/m_B$ denotes the mass-ratio, r/m , Ω_i and \dot{a} denote initial separation, orbital frequency and expansion factor, respectively. χ_A and χ_B are the dimensionless spin components of the first and the second hole, and e_Ω is the orbital eccentricity. The final orbital frequency is given by Ω_f , and N_f denotes the number of orbits N_f between the initial frequency Ω_i and the final frequency Ω_f . The last column denote the number of orbits between the initial orbital frequency until the orbital frequency $0.05/m$.

ScN	q	r/m	χ_A	θ_A/π	ϕ_A/π	χ_B	θ_B/π	ϕ_B/π	$10^2 m\Omega_i$	$10^5 \dot{a}$	$10^4 e_\Omega$	$10^2 m\Omega_f$	N_f	$N_{0.05}$
70	1.07	15	0.205	0.965	0.091	0.385	0.229	-0.185	1.5821	-5.98	0.8	9.5	17.21	15.83
71	1.08	15	0.106	0.400	0.590	0.212	0.340	-0.191	1.5817	-5.40	0.7	13.	17.73	16.00
72	1.08	15	0.154	0.352	-0.364	0.470	0.646	-0.960	1.5838	-4.56	0.2	6.5	16.09	15.37
73	1.10	15	0.494	0.818	-0.028	0.142	0.152	-0.364	1.5854	-5.85	0.5	6.0	15.40	14.88
74	1.12	15	0.269	0.083	0.507	0.076	0.474	-0.061	1.5795	-4.35	0.5	12.	18.18	16.41
75	1.12	15	0.377	0.109	-0.712	0.458	0.725	-0.935	1.5809	-3.45	0.5	8.1	17.18	15.97
76	1.12	15	0.344	0.028	0.492	0.352	0.240	-0.931	1.5761	-2.79	0.5	11.	19.12	17.19
77	1.12	15	0.243	0.517	-0.496	0.269	0.625	-0.792	1.5866	-4.26	2.0	11.	16.91	15.43
78	1.17	15	0.481	0.958	0.542	0.370	0.943	0.220	1.5919	-7.31	2.3	8.6	14.44	13.57
79	1.26	15	0.267	0.415	-0.156	0.311	0.128	-0.386	1.5797	-4.97	1.0	11.	18.42	16.66
80	1.27	15	0.073	0.786	0.362	0.463	0.452	0.106	1.5829	-1.75	0.5	7.5	16.88	15.84
81	1.29	15	0.357	0.424	-0.907	0.452	0.345	0.677	1.5839	-6.09	2.9	7.8	17.82	16.59
82	1.34	15	0.079	0.568	-0.523	0.200	0.853	-0.820	1.5844	-5.45	0.3	11.	16.95	15.53
83	1.35	15	0.140	0.094	-0.122	0.413	0.091	0.430	1.5777	-3.31	0.2	10.	18.91	17.18
84	1.36	15	0.089	0.005	-0.975	0.356	0.568	-0.404	1.5866	-6.51	2.9	11.	17.69	16.09
85	1.38	15	0.169	0.531	-0.097	0.455	0.235	-0.152	1.5799	-5.88	1.0	7.9	17.89	16.67
86	1.55	15	0.082	0.820	-0.171	0.205	0.825	-0.052	1.5847	-5.74	0.4	11.	17.20	15.76
87	1.63	15	0.114	0.521	-0.665	0.325	0.101	-0.587	1.5806	-3.49	1.2	9.8	18.57	17.05
88	1.63	15	0.295	0.516	0.635	0.179	0.060	0.310	1.5832	-5.15	1.7	12.	18.50	16.78
89	1.63	15	0.171	0.786	-0.032	0.155	0.544	-0.983	1.5843	-5.15	0.2	11.	17.46	15.99
90	1.64	15	0.115	0.435	0.808	0.343	0.730	-0.361	1.5861	-6.82	1.4	11.	17.65	16.17
91	1.68	15	0.365	0.148	-0.283	0.217	0.269	-0.911	1.5772	-3.53	0.8	12.	20.04	18.03

Continued

TABLE II – *Continued*

ScN	q	r/m	χ_A	θ_A/π	ϕ_A/π	χ_B	θ_B/π	ϕ_B/π	$10^2 m\Omega_i$	$10^5 \dot{a}$	$10^4 e_\Omega$	$10^2 m\Omega_f$	N_f	$N_{0.05}$
92	1.70	15	0.429	0.470	0.487	0.112	0.958	-0.874	1.5880	-5.20	4.9	12.	18.22	16.60
93	1.76	15	0.406	0.530	-0.810	0.252	0.764	0.476	1.5866	-2.88	1.5	11.	17.79	16.33
94	1.82	15	0.403	0.326	-0.511	0.146	0.590	-0.953	1.5828	-4.13	2.4	11.	19.44	17.67
95	1.82	15	0.438	0.658	-0.446	0.124	0.253	0.690	1.5891	-5.74	2.9	9.5	17.56	16.29
96	1.84	15	0.208	0.364	0.875	0.160	0.420	0.640	1.5815	-4.99	0.9	11.	19.08	17.40
97	1.91	15	0.375	0.545	-0.854	0.110	0.012	-0.107	1.5826	-2.71	0.6	11.	18.76	17.17
98	1.92	15	0.451	0.082	-0.887	0.443	0.563	-0.652	1.5834	+3.02	4.6	8.6	20.34	18.73
99	1.94	15	0.312	0.873	0.292	0.222	0.080	-0.934	1.5853	-4.26	0.8	11.	17.88	16.46
100	1.96	15	0.057	0.810	0.274	0.090	0.408	-0.113	1.5827	-4.68	0.4	12.	18.76	17.14
101	1.97	15	0.190	0.564	-0.917	0.372	0.911	0.727	1.5851	-5.78	0.5	9.5	17.82	16.56

TABLE III: Parameters $a_{i,j}$ of ρ_{NS} .

i	$j=0$	$j=1$	$j=2$	$j=3$
0	-2.23773	89.0053	-907.744	3194.70
1	16.3786	-321.623	1589.74	0
2	-25.8886	285.810	0	0
3	7.94034	0	0	0

TABLE IV: Parameters $b_{i,j}$ of κ_{NS} .

i	$j=0$	$j=1$	$j=2$	$j=3$
0	0.999768	-2.63274	4.08714	-2.67330
1	-0.0126939	0.343292	1.75169	0
2	0.0445636	-0.975111	0	0
3	0.0157333	0	0	0

TABLE V: Parameters $c_{i,j,k}$ of $\delta\kappa_{\text{S}}$.

(i,k)	$j=1$	$j=2$	$j=3$	$j=4$
(0,1)	5316.71	-66338.2	275375.	-380348.
(0,2)	32067.7	-376132.	1.48805×10^6	-1.93024×10^6
(0,3)	14274.6	-177525.	736095.	-1.01733×10^6
(0,4)	-1843.34	9864.44	1329.56	-4958.02
(0,5)	109.978	517.973	-7645.17	15290.1
(0,6)	23169.4	-275526.	1.08011×10^6	-1.42663×10^6
(0,7)	7819.45	-101310.	434622.	-617796.
(0,8)	-42885.3	532586.	-2.20338×10^6	3.03600×10^6
(0,9)	1027.50	-27767.7	103643.	-218964.
(0,10)	-109193.	1.29526×10^6	-5.05535×10^6	6.62736×10^6
(0,11)	-55234.7	704761.	-2.98370×10^6	4.19269×10^6
(0,12)	-92749.8	1.02247×10^6	-4.02065×10^6	5.29669×10^6
(0,13)	-7921.47	97674.7	-405463.	565779.
(0,14)	-103301.	1.22607×10^6	-4.82157×10^6	6.34451×10^6
(1,1)	-82960.2	1.03434×10^6	-4.29063×10^6	5.92217×10^6
(1,2)	-496416.	5.85007×10^6	-2.32014×10^7	3.02622×10^7
(1,3)	-217655.	2.71089×10^6	-1.12563×10^7	1.55773×10^7
(1,4)	25018.3	-393524.	2.05655×10^6	-4.12184×10^6
(1,5)	28030.5	-368855.	1.57451×10^6	-2.19102×10^6
(1,6)	-412124.	4.87348×10^6	-1.90352×10^7	2.49538×10^7
(1,7)	-128584.	1.65610×10^6	-7.06852×10^6	1.00034×10^7
(1,8)	661241.	-8.21574×10^6	3.40040×10^7	-4.68715×10^7
(1,9)	-24548.5	478963.	-1.79194×10^6	3.37544×10^6
(1,10)	1.69467×10^6	-2.01047×10^7	7.86851×10^7	-1.03283×10^8
(1,11)	917140.	-1.16445×10^7	4.90819×10^7	-6.86985×10^7
(1,12)	-289050.	3.65366×10^6	-1.08819×10^7	8.95028×10^6
(1,13)	46482.3	-583937.	2.51586×10^6	-3.69108×10^6
(1,14)	1.74966×10^6	-2.07098×10^7	8.12790×10^7	-1.06573×10^8
(2,1)	424444.	-5.28782×10^6	2.19181×10^7	-3.02304×10^7
(2,2)	2.54951×10^6	-3.01226×10^7	1.19551×10^8	-1.56397×10^8
(2,3)	1.08832×10^6	-1.35750×10^7	5.64446×10^7	-7.82131×10^7
(2,4)	538865.	-4.65423×10^6	1.08665×10^7	-650921.
(2,5)	-134766.	1.75054×10^6	-7.36970×10^6	1.00998×10^7
(2,6)	2.38473×10^6	-2.81363×10^7	1.09819×10^8	-1.43508×10^8
(2,7)	690728.	-8.84984×10^6	3.76020×10^7	-5.30045×10^7
(2,8)	-3.34460×10^6	4.15737×10^7	-1.72135×10^8	2.37354×10^8
(2,9)	149314.	-2.61396×10^6	1.01824×10^7	-1.80892×10^7
(2,10)	-8.70071×10^6	1.03298×10^8	-4.05413×10^8	5.32989×10^8

Continued

TABLE V – *Continued*

(i, k)	$j = 1$	$j = 2$	$j = 3$	$j = 4$
(2,11)	-4.98684×10^6	6.30344×10^7	-2.64631×10^8	3.69064×10^8
(2,12)	362328.	2.89435×10^6	-6.26526×10^7	1.54943×10^8
(2,13)	-296859.	3.76776×10^6	-1.62996×10^7	2.38893×10^7
(2,14)	-9.73227×10^6	1.15044×10^8	-4.51208×10^8	5.90608×10^8
(3,1)	-709184.	8.82898×10^6	-3.65705×10^7	5.04053×10^7
(3,2)	-4.35305×10^6	5.15001×10^7	-2.04343×10^8	2.67729×10^8
(3,3)	-1.78215×10^6	2.22596×10^7	-9.26725×10^7	1.28564×10^8
(3,4)	908964.	-1.60025×10^7	8.51391×10^7	-1.47147×10^8
(3,5)	62120.2	-864159.	3.64740×10^6	-4.74819×10^6
(3,6)	-4.48307×10^6	5.28627×10^7	-2.06464×10^8	2.69548×10^8
(3,7)	-1.20683×10^6	1.53949×10^7	-6.51614×10^7	9.15436×10^7
(3,8)	5.53612×10^6	-6.88414×10^7	2.85135×10^8	-3.93290×10^8
(3,9)	-265327.	4.52185×10^6	-1.85463×10^7	3.22321×10^7
(3,10)	1.48479×10^7	-1.76472×10^8	6.94463×10^8	-9.14535×10^8
(3,11)	8.83120×10^6	-1.11213×10^8	4.65325×10^8	-6.46984×10^8
(3,12)	-6.70535×10^6	5.32904×10^7	-6.84880×10^7	-1.07762×10^8
(3,13)	1.00833×10^6	-1.27036×10^7	5.39248×10^7	-7.69297×10^7
(3,14)	1.77463×10^7	-2.09671×10^8	8.22363×10^8	-1.07571×10^9

TABLE VI: Parameters $d_{i,j,k}$ of $\delta\rho_S$.

(i, k)	$j = 1$	$j = 2$	$j = 3$	$j = 4$
(0,1)	-45382.3	302204.	-153169.	-1.30349×10^6
(0,2)	-253943.	1.90739×10^6	632048.	-7.50294×10^6
(0,3)	-1.31299×10^6	1.54603×10^7	-6.03927×10^7	7.82728×10^7
(0,4)	-1.20248×10^6	8.98755×10^6	-2.09367×10^7	2.51332×10^7
(0,5)	550699.	-6.20436×10^6	2.42440×10^7	-3.28133×10^7
(0,6)	587207.	-7.79345×10^6	3.28891×10^7	-4.78587×10^7
(0,7)	-234908.	2.08401×10^6	-5.31451×10^6	2.96473×10^6
(0,8)	529948.	-4.20533×10^6	7.57153×10^6	2.97058×10^6
(0,9)	677458.	-1.23094×10^7	5.30880×10^7	-9.37766×10^7
(0,10)	4.56142×10^6	-5.15215×10^7	2.05792×10^8	-2.57620×10^8
(0,11)	-5.37955×10^6	8.86716×10^7	-4.55622×10^8	7.47340×10^8
(0,12)	-1.23435×10^7	1.01134×10^8	-3.15628×10^8	3.51274×10^8
(0,13)	-1.45409×10^6	1.69206×10^7	-6.86296×10^7	9.64437×10^7
(0,14)	5.15330×10^6	-5.79718×10^7	2.18460×10^8	-2.69339×10^8
(1,1)	-45382.3	302204.	-153169.	-1.30349×10^6
(1,2)	-253943.	1.90739×10^6	632048.	-7.50294×10^6
(1,3)	-1.31299×10^6	1.54603×10^7	-6.03927×10^7	7.82728×10^7
(1,4)	-1.20248×10^6	8.98755×10^6	-2.09367×10^7	2.51332×10^7
(1,5)	550699.	-6.20436×10^6	2.42440×10^7	-3.28133×10^7
(1,6)	587207.	-7.79345×10^6	3.28891×10^7	-4.78587×10^7
(1,7)	-234908.	2.08401×10^6	-5.31451×10^6	2.96473×10^6
(1,8)	529948.	-4.20533×10^6	7.57153×10^6	2.97058×10^6
(1,9)	677458.	-1.23094×10^7	5.30880×10^7	-9.37766×10^7
(1,10)	4.56142×10^6	-5.15215×10^7	2.05792×10^8	-2.57620×10^8
(1,11)	-5.37955×10^6	8.86716×10^7	-4.55622×10^8	7.47340×10^8
(1,12)	-1.23435×10^7	1.01134×10^8	-3.15628×10^8	3.51274×10^8
(1,13)	-1.45409×10^6	1.69206×10^7	-6.86296×10^7	9.64437×10^7
(1,14)	5.15330×10^6	-5.79718×10^7	2.18460×10^8	-2.69339×10^8
(2,1)	-45382.3	302204.	-153169.	-1.30349×10^6
(2,2)	-253943.	1.90739×10^6	632048.	-7.50294×10^6
(2,3)	-1.31299×10^6	1.54603×10^7	-6.03927×10^7	7.82728×10^7
(2,4)	-1.20248×10^6	8.98755×10^6	-2.09367×10^7	2.51332×10^7
(2,5)	550699.	-6.20436×10^6	2.42440×10^7	-3.28133×10^7
(2,6)	587207.	-7.79345×10^6	3.28891×10^7	-4.78587×10^7
(2,7)	-234908.	2.08401×10^6	-5.31451×10^6	2.96473×10^6
(2,8)	529948.	-4.20533×10^6	7.57153×10^6	2.97058×10^6
(2,9)	677458.	-1.23094×10^7	5.30880×10^7	-9.37766×10^7
(2,10)	4.56142×10^6	-5.15215×10^7	2.05792×10^8	-2.57620×10^8
(2,11)	-5.37955×10^6	8.86716×10^7	-4.55622×10^8	7.47340×10^8
(2,12)	-1.23435×10^7	1.01134×10^8	-3.15628×10^8	3.51274×10^8
(2,13)	-1.45409×10^6	1.69206×10^7	-6.86296×10^7	9.64437×10^7
(2,14)	5.15330×10^6	-5.79718×10^7	2.18460×10^8	-2.69339×10^8

Continued

TABLE VI – *Continued*

(i, k)	$j = 1$	$j = 2$	$j = 3$	$j = 4$
(3,1)	-45382.3	302204.	-153169.	-1.30349 $\times 10^6$
(3,2)	-253943.	1.90739 $\times 10^6$	632048.	-7.50294 $\times 10^6$
(3,3)	-1.31299 $\times 10^6$	1.54603 $\times 10^7$	-6.03927 $\times 10^7$	7.82728 $\times 10^7$
(3,4)	-1.20248 $\times 10^6$	8.98755 $\times 10^6$	-2.09367 $\times 10^7$	2.51332 $\times 10^7$
(3,5)	550699.	-6.20436 $\times 10^6$	2.42440 $\times 10^7$	-3.28133 $\times 10^7$
(3,6)	587207.	-7.79345 $\times 10^6$	3.28891 $\times 10^7$	-4.78587 $\times 10^7$
(3,7)	-234908.	2.08401 $\times 10^6$	-5.31451 $\times 10^6$	2.96473 $\times 10^6$
(3,8)	529948.	-4.20533 $\times 10^6$	7.57153 $\times 10^6$	2.97058 $\times 10^6$
(3,9)	677458.	-1.23094 $\times 10^7$	5.30880 $\times 10^7$	-9.37766 $\times 10^7$
(3,10)	4.56142 $\times 10^6$	-5.15215 $\times 10^7$	2.05792 $\times 10^8$	-2.57620 $\times 10^8$
(3,11)	-5.37955 $\times 10^6$	8.86716 $\times 10^7$	-4.55622 $\times 10^8$	7.47340 $\times 10^8$
(3,12)	-1.23435 $\times 10^7$	1.01134 $\times 10^8$	-3.15628 $\times 10^8$	3.51274 $\times 10^8$
(3,13)	-1.45409 $\times 10^6$	1.69206 $\times 10^7$	-6.86296 $\times 10^7$	9.64437 $\times 10^7$
(3,14)	5.15330 $\times 10^6$	-5.79718 $\times 10^7$	2.18460 $\times 10^8$	-2.69339 $\times 10^8$

-
- [1] *Advanced ligo*, <http://lhocds.ligo-wa.caltech.edu:8000/advligo/GWINC>.
- [2] L. scientific collaboration, *The science of lsc research*, URL <http://www.ligo.org/science/overview.php>.
- [3] J. Abadie et al. (The LIGO Scientific Collaboration and the Virgo Collaboration, the Virgo Collaboration) (2012), 1201.5999.
- [4] F. Acernese, M. Alshourbagy, P. Amico, F. Antonucci, S. Aoudia, et al., *Class.Quant.Grav.* **25**, 184001 (2008).
- [5] K. Somiya and the KAGRA Collaboration, *Class. Quantum Grav.* **29**, 124007 (2012).
- [6] F. Pretorius, *Class. Quantum Grav.* **22**, 425 (2005).
- [7] J. Centrella, J. G. Baker, B. J. Kelly, and J. R. van Meter, *Rev. Mod. Phys.* **82**, 3069 (2010).
- [8] H. P. Pfeiffer, *Numerical simulations of compact object binaries* (2012), 1203.5166.
- [9] A. Buonanno, Y. Pan, J. G. Baker, J. Centrella, B. J. Kelly, et al., *Phys. Rev. D* **76**, 104049 (2007), 0706.3732.
- [10] P. Ajith, S. Babak, Y. Chen, M. Hewitson, B. Krishnan, et al., *Phys. Rev. D* **77**, 104017 (2008), 0710.2335.
- [11] T. Damour and A. Nagar, *Phys. Rev. D* **79**, 081503 (2009), 0902.0136.
- [12] A. Buonanno, Y. Pan, H. P. Pfeiffer, M. A. Scheel, L. T. Buchman, et al., *Phys. Rev. D* **79**, 124028 (2009), 0902.0790.
- [13] P. Ajith, M. Hannam, S. Husa, Y. Chen, B. Brügmann, N. Dorband, D. Mueller, F. Ohme, D. Pollney, C. Reisswig, et al. (2009), 0909.2867.
- [14] Y. Pan, A. Buonanno, L. T. Buchman, T. Chu, L. E. Kidder, et al., *Phys.Rev.* **D81**, 084041 (2010), 0912.3466.
- [15] B. Aylott et al., *Class. Quantum Grav.* **26**, 165008 (2009).
- [16] L. Santamaría, F. Ohme, P. Ajith, B. Brügmann, N. Dorband, M. Hannam, S. Husa, P. Mösta, D. Pollney, C. Reisswig, et al., *Phys. Rev. D* **82**, 064016 (2010).
- [17] P. Ajith, M. Boyle, D. A. Brown, B. Brügmann, L. T. Buchman, et al., *Class. Quantum Grav.* **29**, 124001 (2012), URL <http://stacks.iop.org/0264-9381/29/i=12/a=124001>.
- [18] B. Aylott, J. G. Baker, W. D. Boggs, M. Boyle, P. R. Brady, et al., *Class.Quant.Grav.* **26**, 165008 (2009), 0901.4399.
- [19] P. C. Peters and J. Mathews, *Phys. Rev.* **131**, 435 (1963).
- [20] P. C. Peters, *Phys. Rev.* **136**, B1224 (1964).
- [21] F. Ohme, *Class.Quant.Grav.* **29**, 124002 (2012), 1111.3737.
- [22] J. G. Baker, S. T. McWilliams, J. R. van Meter, J. Centrella, D.-I. Choi, B. J. Kelly, and M. Koppitz, *Phys. Rev. D* **75**, 124024 (2007).
- [23] B. Brügmann, J. A. González, M. Hannam, S. Husa, U. Sperhake, and W. Tichy, *Phys. Rev. D* **77**, 024027 (2008).
- [24] M. Campanelli, C. Lousto, P. Marronetti, and Y. Zlochower, *Phys.Rev.Lett.* **96**, 111101 (2006), gr-qc/0511048.
- [25] M. Campanelli, C. O. Lousto, and Y. Zlochower, *Phys. Rev. D* **74**, 041501(R) (2006), gr-qc/0604012.
- [26] S. Husa, J. A. González, M. Hannam, B. Brügmann, and U. Sperhake, *Class. Quantum Grav.* **25**, 105006 (2008).
- [27] L. Boyle, M. Kesden, and S. Nissanke, *Phys. Rev. Lett.* **100**, 151101 (2008), arXiv:0709.0299 [gr-qc].
- [28] J. G. Baker, M. Campanelli, F. Pretorius, and Y. Zlochower, *Class. Quantum Grav.* **24**, S25 (2007).
- [29] T. Bode, D. Shoemaker, F. Herrmann, and I. Hinder, *Phys. Rev. D* **77**, 44027 (2008).
- [30] T. Chu, H. P. Pfeiffer, and M. A. Scheel, *Phys. Rev. D* **80**, 124051 (2009), 0909.1313.
- [31] M. A. Scheel, M. Boyle, T. Chu, L. E. Kidder, K. D. Matthews and H. P. Pfeiffer, *Phys. Rev. D* **79**, 024003 (2009), arXiv:gr-qc/0810.1767.
- [32] M. Hannam, S. Husa, J. G. Baker, M. Boyle, B. Brügmann, T. Chu, N. Dorband, F. Herrmann, I. Hinder, B. J. Kelly, et al., *Phys. Rev. D* **79**, 084025 (2009), arXiv:0901.2437.
- [33] G. Lovelace, M. Scheel, and B. Szilagyi, *Phys. Rev. D* **83**, 024010 (2011), 1010.2777.
- [34] M. Hannam, S. Husa, F. Ohme, D. Müller, and B. Brügmann, *Phys. Rev. D* **82**, 124008 (2010), arXiv:1007.4789.
- [35] G. Lovelace, M. Boyle, M. A. Scheel, and

- B. Szilágyi, *Class. Quant. Grav.* **29**, 045003 (2012), arXiv:1110.2229.
- [36] L. T. Buchman, H. P. Pfeiffer, M. A. Scheel, and B. Szilágyi, *Simulations of unequal mass binary black holes with spectral methods* (2012), 1206.3015.
- [37] M. Hannam, S. Husa, F. Ohme, and P. Ajith, *Phys. Rev. D* **82**, 124052 (2010).
- [38] P. Ajith, S. Babak, Y. Chen, M. Hewitson, B. Krishnan, A. M. Sintes, J. T. Whelan, B. Brügmann, P. Diener, N. Dorband, et al., *Phys. Rev. D* **79**, 129901 (2009).
- [39] P. Ajith, M. Hannam, S. Husa, Y. Chen, B. Bruegmann, N. Dorband, D. Mueller, F. Ohme, D. Pollney, C. Reisswig, et al., *ArXiv e-prints* (2009), 0909.2867.
- [40] A. L. Tiec, A. H. Mroué, L. Barack, A. Buonanno, H. P. Pfeiffer, et al., *Phys. Rev. Lett.* **107**, 141101 (2011), 1106.3278.
- [41] A. H. Mroué, L. E. Kidder, and S. A. Teukolsky, *Phys. Rev. D* **78**, 044004 (2008).
- [42] A. Taracchini, A. Buonanno, E. Barausse, M. Boyle, T. Chu, G. Lovelace, H. P. Pfeiffer, and M. A. Scheel (2012), 1202.0790.
- [43] M. Boyle, A. Buonanno, L. E. Kidder, A. H. Mroué, Y. Pan, et al., *Phys. Rev. D* **78**, 104020 (2008), 0804.4184.
- [44] Y. Pan, A. Buonanno, M. Boyle, L. T. Buchman, L. E. Kidder, H. P. Pfeiffer, and M. A. Scheel, *Phys. Rev. D* **84**, 124052 (2011), 1106.1021.
- [45] M. Campanelli, C. O. Lousto, Y. Zlochower, and D. Merritt, *Astrophys. J. Lett.* **659**, L5 (2007).
- [46] M. Campanelli, C. O. Lousto, Y. Zlochower, B. Krishnan, and D. Merritt, *Phys. Rev. D* **75**, 064030 (2007), gr-qc/0612076.
- [47] P. Schmidt, M. Hannam, S. Husa, and P. Ajith, *Phys. Rev. D* **84**, 024046 (2011), arxiv:1012.2879.
- [48] O'Shaughnessy, R. and Vaishnav, B. and Healy, J. and Meeks, Z. and Shoemaker, D., *Efficient asymptotic frame selection for binary black hole spacetimes using asymptotic radiation* (2011), arXiv:1109.5224.
- [49] M. Boyle, R. Owen, and H. P. Pfeiffer, *Phys. Rev. D* **84**, 124011 (2011), arXiv:1110.2965.
- [50] R. Sturani, S. Fischetti, L. Cadonati, G. Guidi, J. Healy, et al. (2010), 1012.5172.
- [51] R. Sturani, S. Fischetti, L. Cadonati, G. Guidi, J. Healy, et al., *J. Phys. Conf. Ser.* **243**, 012007 (2010), 1005.0551.
- [52] R. O'Shaughnessy, J. Healy, L. London, Z. Meeks, and D. Shoemaker, *Phys. Rev. D* **85**, 084003 (2012), 1201.2113.
- [53] A. Buonanno, G. B. Cook, and F. Pretorius, *Phys. Rev. D* **75**, 124018 (2007), gr-qc/0610122.
- [54] H. P. Pfeiffer, D. A. Brown, L. E. Kidder, L. Lindblom, G. Lovelace, and M. A. Scheel, *Class. Quantum Grav.* **24**, S59 (2007).
- [55] J. G. Baker, J. R. van Meter, S. T. McWilliams, J. Centrella, and B. J. Kelly, *Phys. Rev. Lett.* **99**, 181101 (2007).
- [56] C. Lincoln and C. Will, *Phys. Rev. D* **42**, 1123 (1990).
- [57] T. Damour and G. Schäfer, *Nuovo Cimento Soc. Ital. Fis.* **101 B**, 127 (1988).
- [58] T. Damour, A. Gopakumar, and B. R. Iyer, *Phys. Rev. D* **70**, 064028 (2004).
- [59] C. Königsdörffer and A. Gopakumar, *Phys. Rev. D* **73**, 124012 (2006), gr-qc/0603056.
- [60] R. M. Memmesheimer, A. Gopakumar and G. Schäfer, *Phys. Rev. D* **70**, 104011 (2004).
- [61] E. Berti, S. Iyer, and C. M. Will, *Phys. Rev. D* **74**, 061503 (2006), gr-qc/0607047.
- [62] T. Mora and C. Will, *Phys. Rev. D* **66**, 101501(R) (2002).
- [63] S. Husa, M. Hannam, J. A. González, U. Sperhake, and B. Brügmann, *Phys. Rev. D* **77**, 044037 (2008), 0706.0904.
- [64] M. Campanelli, C. O. Lousto, H. Nakano, and Y. Zlochower, *Phys. Rev. D* **79**, 84010 (2009), arXiv:gr-qc/0808.0713.
- [65] A. H. Mroué, H. P. Pfeiffer, L. E. Kidder, and S. A. Teukolsky, *Phys. Rev. D* **82**, 124016 (2010), arXiv:1004.4697 [gr-qc].
- [66] A. Buonanno, L. E. Kidder, A. H. Mroué, H. P. Pfeiffer, and A. Taracchini, *Phys. Rev. D* **83**, 104034 (2011), 1012.1549.
- [67] M. Boyle, D. A. Brown, L. E. Kidder, A. H. Mroué, H. P. Pfeiffer, M. A. Scheel, G. B. Cook, and S. A. Teukolsky, *Phys. Rev. D* **76**, 124038 (2007).
- [68] W. Tichy and P. Marronetti (2010), 1010.2936.
- [69] M. Purrer, S. Husa, and M. Hannam, *Phys. Rev. D* **85**, 124051 (2012), 1203.4258.
- [70] L. T. Buchman, H. P. Pfeiffer, M. A. Scheel, and B. Szilágyi, *Simulations of non-equal mass black hole binaries, in preparation.*
- [71] D. Brown and P. Zimmerman., *Phys. Rev. D* **81**, 024007 (2010), arXiv:gr-qc/0909.0066.
- [72] J. W. York, *Phys. Rev. Lett.* **82**, 1350 (1999).
- [73] H. P. Pfeiffer and J. W. York, *Phys. Rev. D* **67**, 044022 (2003).
- [74] G. B. Cook, *Phys. Rev. D* **65**, 084003 (2002).
- [75] G. B. Cook and H. P. Pfeiffer, *Phys. Rev. D* **70**, 104016 (2004).
- [76] M. Caudill, G. B. Cook, J. D. Grigsby, and H. P. Pfeiffer, *Phys. Rev. D* **74**, 064011 (2006).
- [77] H. P. Pfeiffer, L. E. Kidder, M. A. Scheel, and S. A. Teukolsky, *Comput. Phys. Commun.* **152**, 253 (2003).
- [78] <http://www.black-holes.org/SpEC.html>.
- [79] L. Lindblom, M. A. Scheel, L. E. Kidder, R. Owen, and O. Rinne, *Class. Quantum Grav.* **23**, S447 (2006).
- [80] H. Friedrich, *Commun. Math. Phys.* **100**, 525 (1985).
- [81] D. Garfinkle, *Phys. Rev. D* **65**, 044029 (2002).
- [82] C. Gundlach, J. M. Martin-Garcia, G. Calabrese, and I. Hinder, *Class. Quantum Grav.* **22**, 3767 (2005).
- [83] O. Rinne, *Class. Quantum Grav.* **23**, 6275 (2006).
- [84] O. Rinne, L. Lindblom, and M. A. Scheel, *Class. Quantum Grav.* **24**, 4053 (2007).
- [85] J. M. Stewart, *Class. Quantum Grav.* **15**, 2865 (1998).
- [86] H. Friedrich and G. Nagy, *Commun. Math. Phys.* **201**, 619 (1999).
- [87] J. M. Bardeen and L. T. Buchman, *Phys. Rev. D* **65**, 064037 (2002).
- [88] B. Szilágyi, B. Schmidt, and J. Winicour, *Phys. Rev. D* **65**, 064015 (2002).
- [89] G. Calabrese, J. Pullin, O. Reula, O. Sarbach, and M. Tiglio, *Commun. Math. Phys.* **240**, 377 (2003), gr-qc/0209017.
- [90] B. Szilágyi and J. Winicour, *Phys. Rev. D* **68**, 041501(R) (2003).
- [91] L. E. Kidder, L. Lindblom, M. A. Scheel, L. T. Buchman, and H. P. Pfeiffer, *Phys. Rev. D* **71**, 064020 (2005).
- [92] L. T. Buchman and O. C. A. Sarbach, *Class. Quantum Grav.* **23**, 6709 (2006).
- [93] L. T. Buchman and O. C. A. Sarbach, *Class. Quantum*

- Grav. **24**, S307 (2007).
- [94] D. Gottlieb and J. S. Hesthaven, J. Comput. Appl. Math. **128**, 83 (2001), ISSN 0377-0427.
 - [95] J. S. Hesthaven, Appl. Num. Math. **33**, 23 (2000).
 - [96] S. Ossokine, L. E. Kidder, and H. P. Pfeiffer, *Precession-tracking coordinates for binary black hole simulations*, in preparation.
 - [97] B. Szilagyi, L. Lindblom, and M. A. Scheel, Phys. Rev. D **80**, 124010 (2009), 0909.3557.
 - [98] L. E. Kidder, Phys. Rev. D **52**, 821 (1995).
 - [99] B. Garcia, G. Lovelace, L. E. Kidder, M. Boyle, S. A. Teukolsky, et al. (2012), 1206.2943.
 - [100] G. Lovelace, R. Owen, H. P. Pfeiffer, and T. Chu, Phys. Rev. D **78**, 084017 (2008).
 - [101] G. Lovelace, Class. Quantum Grav. **26**, 114002 (2009).